Journal of Pharmaceutical Analysis 15 (2025) 101069

Contents lists available at ScienceDirect

Journal of Pharmaceutical Analysis

journal homepage: www.elsevier.com/locate/jpa

Original article

New applications of clioquinol in the treatment of inflammation disease by directly targeting arginine 335 of NLRP3

Peipei Chen [a, b, c, d], Yunshu Wang [a, b, c, d], Huaiping Tang [a, b, c, d], Chao Zhou [a, b, c, d], Zhuo Liu [a, b, c, d], Shenghan Gao [a, b, c, d], Tingting Wang [e, ***], Yun Xu [a, b, c, d, **], Sen-Lin Ji [a, b, c, d, *]

[a] Department of Neurology, Nanjing Drum Tower Hospital, Affiliated Hospital of Medical School, Nanjing University, Nanjing, 210008, China
[b] State Key Laboratory of Pharmaceutical Biotechnology and Institute of Translational Medicine for Brain Critical Diseases, Nanjing University, Nanjing, 210093, China
[c] Jiangsu Key Laboratory for Molecular Medicine, Medical School of Nanjing University, Nanjing, 210008, China
[d] Nanjing Neurology Clinical Medical Center, Nanjing, 210000, China
[e] State Key Laboratory of Pharmaceutical Biotechnology, Chemistry and Biomedicine Innovation Center (ChemBIC), Jiangsu Key Laboratory of Molecular Medicine, Division of Immunology, Medical School, Nanjing University, Nanjing, 210008, China

ARTICLE INFO

Article history:
Received 9 May 2024
Received in revised form
5 August 2024
Accepted 10 August 2024
Available online 18 August 2024

Keywords:
Clioquinol
NLRP3 inflammasome
NACHT domain
Sepsis
Peritonitis
Colitis

ABSTRACT

The NOD-like receptor protein 3 (NLRP3) inflammasome is essential in innate immune-mediated inflammation, with its overactivation implicated in various autoinflammatory, metabolic, and neurodegenerative diseases. Pharmacological inhibition of NLRP3 offers a promising treatment strategy for inflammatory conditions, although no medications targeting the NLRP3 inflammasome are currently available. This study demonstrates that clioquinol (CQ), a clinical drug with chelating properties, effectively inhibits NLRP3 activation, resulting in reduced cytokine secretion and cell pyroptosis in both human and mouse macrophages, with a half maximal inhibitory concentration (IC_{50}) of 0.478 μM. Additionally, CQ mitigates experimental acute peritonitis, gouty arthritis, sepsis, and colitis by lowering serum levels of interleukin-1β (IL-1β), IL-6, and tumor necrosis factor-α (TNF-α). Mechanistically, CQ covalently binds to Arginine 335 (R335) in the NACHT domain, inhibiting NLRP3 inflammasome assembly and blocking the interaction between NLRP3 and its component protein. Collectively, this study identifies CQ as an effective natural NLRP3 inhibitor and a potential therapeutic agent for NLRP3-driven diseases.

1. Introduction

The NOD-like receptor protein 3 (NLRP3) inflammasome, a polymeric protein complex, is instrumental in regulating cellular immune responses. Its primary components include NLRP3, apoptosis-associated speck-like protein containing a caspase activation and recruitment domain (CARD) domain (ASC) [1], and the precursor form of the proinflammatory cytokine interleukin-1β (IL-1β) [2]. Activation of the NLRP3 inflammasome, triggered by cellular damage or infection, results in the release of pro-inflammatory cytokines that initiate an inflammatory response [3]. The underlying activation mechanism of the NLRP3 inflammasome is complex [4], involving intracellular signals such as elevated calcium ion concentration, oxidative stress, and environmental alterations [2]. These signals prompt conformational changes in NLRP3, enabling its interaction with ASC to form the active inflammasome complex. This complex subsequently activates caspase-1, which then facilitates the maturation and secretion of IL-1β. IL-1β, a pivotal pro-inflammatory factor, triggers immune responses and attracts immune cells to infection sites. Proper NLRP3 inflammasome function is vital for maintaining immune homeostasis and responding to infections. However, its excessive or aberrant activation can lead to diseases such as sepsis, type 2 diabetes, atherosclerosis, inflammatory bowel disease (IBD), and rheumatoid arthritis [5].

* Corresponding author. Department of Neurology, Nanjing Drum Tower Hospital, Affiliated Hospital of Medical School, Nanjing University, Nanjing, 210008, China.
** Corresponding author. Department of Neurology, Nanjing Drum Tower Hospital, Affiliated Hospital of Medical School, Nanjing University, Nanjing, 210008, China.
*** Corresponding author.
E-mail addresses: Cpp20000521@163.com (P. Chen), wswys886@163.com (Y. Wang), 21707050@zju.edu.cn (H. Tang), zhouchao@njglyy.com (C. Zhou), aliceliuzhuo@163.com (Z. Liu), 897172226@qq.com (S. Gao), wangtt@nju.edu.cn (T. Wang), xuyun@nju.edu.cn (Y. Xu), senlinji@njglyy.com (S.-L. Ji).
Peer review under responsibility of Xi'an Jiaotong University.

https://doi.org/10.1016/j.jpha.2024.101069

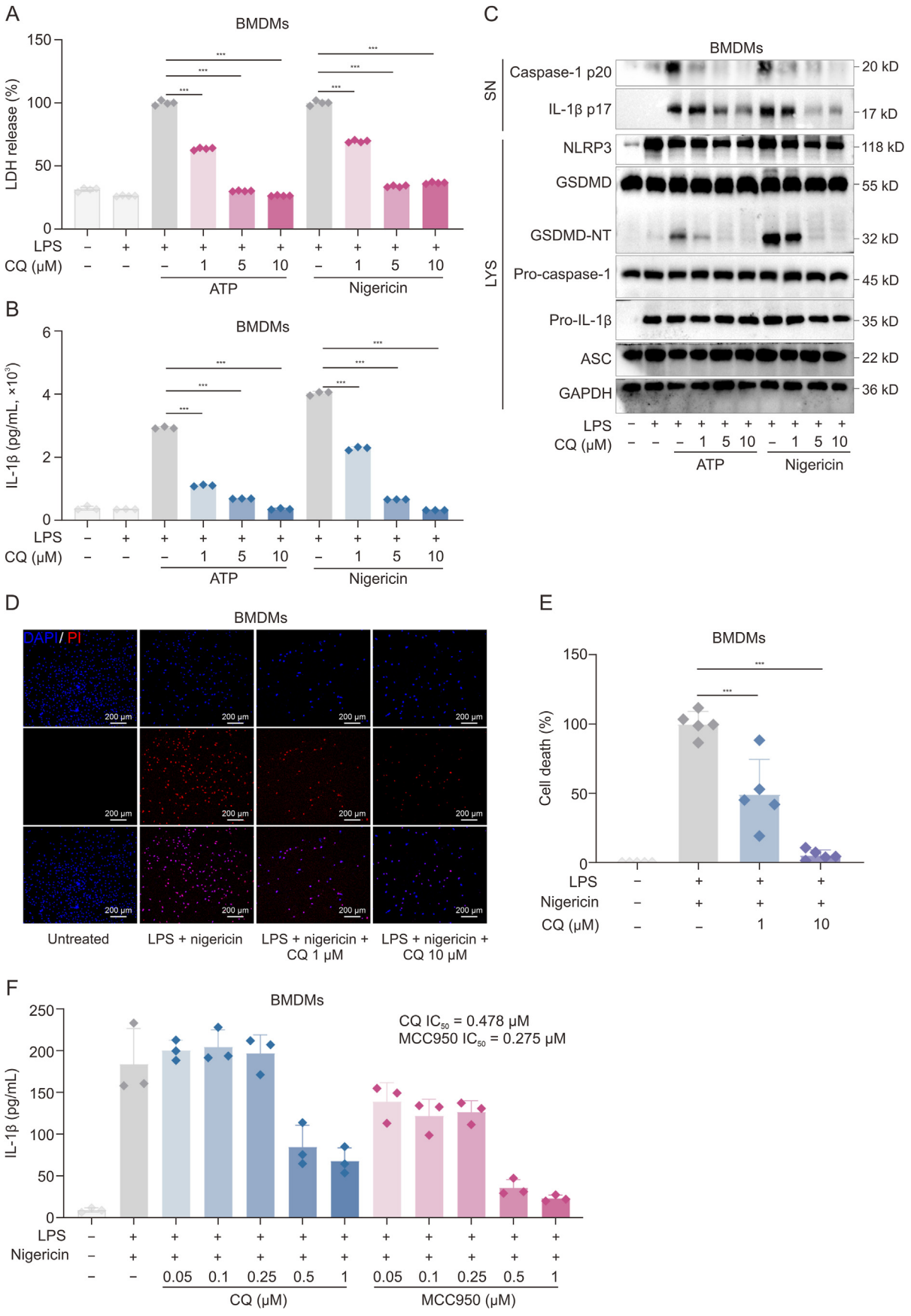

Fig. 1. Clioquinol (CQ) effectively inhibits pyroptosis in mouse macrophages. Lipopolysaccharide (LPS)-primed bone marrow-derived macrophage (BMDM) cells were incubated with different doses of CQ for 1 h and then stimulated with adenosinetriphosphate (ATP) (30 min) or nigericin (60 min). (A) Lactate dehydrogenase (LDH) release in cell supernatant

Pyroptosis, a distinct form of programmed cell death, significantly contributes to inflammatory diseases. Activation of NLRP3 by adenosine triphosphate (ATP), nigericin, or monosodium urate (MSU) forms an inflammasome that activates and cleaves caspase-1 to caspase-1 p20. Activated caspase-1 cleaves gasdermin D (GSDMD), IL-1β, and IL-18, leading to cellular pore formation and pro-inflammatory responses, ultimately inducing pyroptosis [5]. Previous research indicates that inhibiting NLRP3 activation and cell pyroptosis holds significant therapeutic potential for treating inflammatory diseases. MCC950, the first compound specifically known to inhibit the NLRP3 inflammasome, has shown substantial therapeutic benefits in mouse models [6]. Tranilast prevents inflammasome activation by targeting NACHT and inhibiting NLRP3 self-oligomerization [7,8]. Nonetheless, challenges remain in studying the inhibition of the NLRP3 inflammasome and pyroptosis: 1) Current compounds exhibit suboptimal inhibitory effects, necessitating further exploration to identify more effective drugs; 2) Toxic side effects and long-term safety require comprehensive investigation; 3) The precise mechanisms by which many drugs inhibit the NLRP3 inflammasome and pyroptosis remain unclear, warranting further study.

Clioquinol (5-chloro-7-iodo-8-hydroxyquinoline, CQ), a cell-penetrating chelating agent, binds copper and zinc ions and exhibits diverse pharmacological properties, including anti-inflammatory effects [9]. Animal studies have shown CQ's effectiveness in treating fibrosis and neurological diseases [6,10,11]. Recent research indicates that CQ can alleviate pulmonary fibrosis by inactivating fibroblasts, potentially targeting the mechanistic target of rapamycin (mTOR) signalling pathway through iron chelation [12]. Treatment with CQ reduces Huntington protein aggregates, enhances behavioral performance, and extends lifespan in transgenic Huntington's disease mice [10]. Additionally, CQ induces zinc-dependent autophagy, aiding aggregate clearance in astrocytes and neurons, and chelates amyloid beta (Aβ) plaques, potentially reducing Aβ burden by inducing autophagy [13]. Clinical trials suggest that CQ may slow cognitive decline in patients with Alzheimer's disease (AD) by chelating copper and zinc ions [14]. Despite these findings, the molecular mechanisms influenced by CQ remain poorly understood. Some studies suggest that CQ's pharmacological effects may involve interference with mitochondrial function, regulation of oxidative stress response, or modulation of calcium ion homeostasis. However, the precise anti-inflammatory mechanism and targets of CQ are still unknown.

This study identifies CQ as a potent NLRP3 inhibitor through covalent binding to the arginine 335 (R335) residue of the NACHT domain. CQ significantly reduces pyroptosis-induced inflammatory responses, including lactate dehydrogenase release, mature interleukin-1 production, and cleavage of GSDMD, caspase-1 p20, and IL-1β p17. Furthermore, we compared CQ's therapeutic effects with MCC950 (a classical NLRP3 inhibitor) in mouse models of NLRP3-related diseases, such as acute peritonitis, MSU-induced gouty arthritis, lipopolysaccharide (LPS)-induced sepsis, and dextran sulfate sodium salt (DSS)-induced ulcerative colitis (UC). These results underscore CQ's potent inhibitory activity against NLRP3 and its potential for developing novel inhibitors. Repurposing existing drugs also offers significant economic value and enhanced benefits for clinical applications.

2. Materials and methods

2.1. CQ application

CQ (#S4601; Selleck, Houston, TX, USA) was dissolved with dimethyl sulfoxide (DMSO) (ST038, Beyotime, Shanghai, China) to obtain a 50 mg/mL stock solution and further diluted with DMSO to prepare a working solution for *in vitro* use. For *in vivo* animal experiments, CQ stock solution was further diluted to 0.5 or 1 mg/mL with vehicle solution (CQ:PEG300:Tween80 = 1:8:1 (*V/V/V*)) and intraperitoneally injected into experimental mice (5 mg/kg or 10 mg/kg).

2.2. Animals

C57BL/6 mice were procured from the Model Animal Research Center of Nanjing University, while the GSDMD$^{-/-}$ mice were sourced from Cyagen, and the NLRP3$^{-/-}$ mice from Hangzhou Ziyuan Laboratory Animal Technology Co., Ltd. C57BL/6 mice were maintained in a specific pathogen-free (SPF) facility, accredited by the Association for Assessment and Accreditation of Laboratory Animal Care International. All animal experiments were conducted in compliance with the Animal Research: Reporting of *In Vivo* Experiments guidelines and approved by the Animal Care Committee of Nanjing Drum Tower Hospital (Approval No.: 2023AE01029).

2.3. Cell culture

Immortalized bone marrow-derived macrophages (iBMDMs), Tohoku Hospital Pediatrics-1 (THP-1; THP-1 ATCC ® TIB-202™) and Human Embryonic Kidney 293 Cells (HEK-293T; ATCC, CRL-11268) were obtained from ATCC (Manassas, VA, USA). iBMDMs were cultured in high glucose Dulbecco's modified Eagle medium (DMEM; 31985-070, Gibco, Grand Island, NY, USA) and THP-1 cells were cultured in Roswell Park Memorial Institute-1640 (RPMI 1640 medium; 11875119, Gibco). Bone marrow-derived macrophages (BMDMs) were cultured in high-glucose DMEM mixed with 30% L929 cell supernatants (10% day 1, 10% day 2, 10% day 3). All types of cell media should be mixed with 10% fetal bovine serum (FBS; 10091141, Gibco) and 1% penicillin/streptomycin (P/S) (15640055, Gibco). All cells were incubated in cell incubators maintained at 37 °C and 5% CO_2 for growth.

Transfection of HEK-293T cells: HEK-293T cells were transfected with plasmids using Lipo3000 (L3000150, Invitrogen, Carlsbad, CA, USA) for 24–36 h. Post-transfection, varying doses of CQ were administered to the culture dishes, and samples were collected after 8 h. Plasmids were purchased from Wuhan Miaoling Biotechnology Co., Ltd. (Wuhan, China). Plasmids and lentivirus of NLRP3 wild type and mutant (R335A and R335K) were produced from Nanjing Corues Biotechnology Co., Ltd. (Nanjing, China).

2.4. BMDMs differentiation

Primary BMDMs were isolated following established protocols. Briefly, 8–10-week-old C57BL/6 mice were euthanized and submerged in 75% ethanol for 5 min. Bone marrow cells were harvested from the femur and tibia, and cultured in induced DMEM

(SN) of BMDMs. (B) Interleukin-1 beta (IL-1β) production in SN of BMDMs was measured via enzyme-linked immunosorbent assay (ELISA). (C) Western blotting assay for IL-1β p17 and caspase-1 p20 levels in culture SN and NOD-like receptor protein 3 (NLRP3), pro-caspase-1, pro-IL-1β, gasdermin D (GSDMD) (GSDMD-NT) and apoptosis-associated speck-like protein containing a caspase activation and recruitment domain (CARD) (ASC) in lysates (LYS) of BMDMs. (D) NLRP3-activated BMDMs were stained with propidium iodide (PI) (red, dead cells) and 4′,6-diamidino-2-phenylindole (DAPI) (blue, all cells) for 15–20 min, and then observed by fluorescence microscopy. (E)Quantification of dead cells by software ImageJ ($n = 5$). (F) ELISA assay of IL-1β in SN of BMDMs treated with CQ or MCC950 to evaluate half maximal inhibitory concentration (IC_{50}). Data are representative of $n = 4$ (A), $n = 3$ (B, F), $n = 5$ (E) and are expressed as mean ± standard deviation (SD). $^{***}P < 0.001$, determined by one-way analysis of variance (ANOVA) with a Tukey test (relative to LPS + ATP/nigericin). Glyceraldehyde phosphate dehydrogenase (GAPDH) served as a loading control in (C).

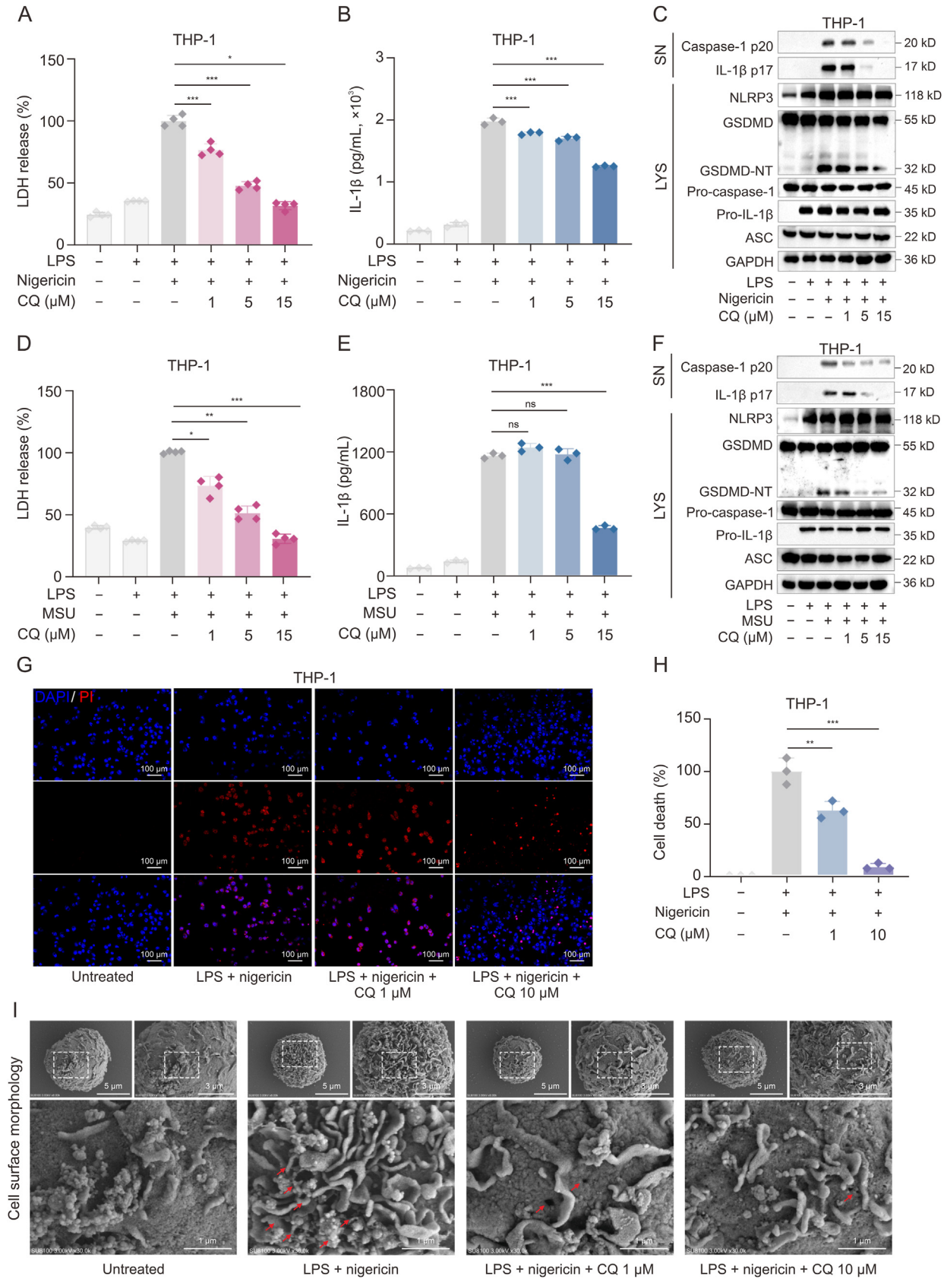

Fig. 2. Clioquinol (CQ) showed significant anti-pyroptosis ability in human macrophages. Lipopolysaccharide (LPS)-primed human monocyte leukemia cells (THP-1) were incubated with different doses of CQ for 1 h and then stimulated with nigericin (90 min) or monosodium urate (MSU) (8 h). (A, D) Lactate dehydrogenase (LDH) release in cell supernatant (SN) of THP-1 cells. LPS + nigericin (A), and LPS + MSU (D). (B, E) Interleukin-1 beta (IL-1β) production in SN of THP-1 cells was measured via enzyme-linked immunosorbent assay (ELISA). LPS + nigericin (B), and LPS + MSU (E). (C, F) Western blotting assay for IL-1β p17 and caspase-1 p20 levels in culture SN and NOD-like receptor protein 3 (NLRP3), pro-

medium. On the third day, half of the medium was replaced with fresh medium. After a 7-day of differentiation period, BMDMs were gently scraped, centrifuged at 1,500 *g*, transferred to 6-well plates overnight, and subsequently treated with CQ or vehicle. The differentiation status of BMDMs was assessed the following day.

2.5. Induction of inflammasome

NLRP3 inflammasome: Cells were pre-incubated with 200 ng/mL LPS (L2630, Sigma-Aldrich, St. Louis, MO, USA) for 3 h, followed by treatment with varying concentrations of CQ for 1 h. The cells were then stimulated ATP (A6419, Sigma-Aldrich) under the following conditions to activate the NLRP3 inflammasome: (1) 4 mmol/L ATP for 30 min; (2) 10 mmol/L nigericin (481990, Sigma-Aldrich) for 1.5–2.5 h; and (3) 0.2 g/L MSU (Tlrl-MSU, Invitrogen) for 6–8 h to induce MSU-activated NLRP3 inflammasome.

Poly(deoxythymidylic-deoxyadenylic) acid (Poly (dA: dT))-activated absent in melanoma 2 (AIM2) inflammasome: Cells were transfected with 0.1 mg/L Poly (dA: dT) (47945S, Cell Signaling Technology, Danvers, MA, USA) using Lipofectamine™ 3000 (L3000075, Invitrogen) for 2.5–4 h after LPS priming and CQ treatment.

Flagellin-activated nucleotide-binding oligomerization domain (NLRC4) inflammasome: Cells were transfected with 0.1 mg/L flagellin (P7388, Beyotime) using Lipofectamine™ 3000 for 6–8 h after LPS priming and CQ treatment.

2.6. Lactate dehydrogenase (LDH) release assay

Cellular LDH content was measured to assess cell death using an LDH assay kit (C10007, Beyotime, Shanghai, China) according to the manufacturer's instructions. Briefly, post-stimulation, the cell supernatant was collected and 60 μL was pipetted into a 96-well plate. Subsequently, 30 μL of the determination mixture was added to the 96-well plate and incubated at 37 °C for 30 min in the dark. Absorbance was measured at 490 nm.

2.7. Cell Counting Kit-8 (CCK8) assay

The CCK8 cell viability assay kit (C0039, Beyotime) was employed to determine the cytotoxicity of CQ following the manufacturer's instructions. Briefly, cells were treated with different concentrations of CQ at 4 h intervals. Subsequently, cells were incubated in the CCK8 reaction solution in the dark at 37 °C for 1–4 h. Absorbance was measured using CytoTox 96 Non-Radioactive kit at 450 nm (≥4 replicates/group).

2.8. 4′,6-Diamidino-2-phenylindole (DAPI)/propidium iodide (PI) staining

To determine the degree of cell death, the DAPI (BD5010, Bioworld, Nanjing, China)/PI (C542, Dojindo, Kumamoto, Japan) staining was conducted to examine living and dead cells. Briefly, the cells were incubated in a 12-well plate overnight and followed with CQ treatment and inflammasome induction. Afterward, the cells were washed with phosphate-buffered saline (PBS)3 times, incubated with DAPI/PI mixture (diluted with DMEM) at room temperature for 10–15 min, washed with PBS for 3 times, fixed with 4% paraformaldehyde (PFA) at 37 °C for 30 min, and observed with an Olympus confocal microscopy (FV3000, Olympus, Tokyo, Japan). 3–5 randomly selected images were taken and analyzed with ImageJ software.

2.9. Western blotting

The cells or tissues were lysed in NP-40 lysis buffer (P0013F, Beyotime) containing 2% phenylmethylsulfonyl fluoride (PMSF; ST506, Beyotime) on ice for 30 min. Protein concentration was measured by the BCA Protein Assay Kit (BD0028, Bioworld) according to the manufacturer's instructions. The lysates were then mixed with either sodium dodecyl sulfate-polyacrylamide gel electrophoresis (SDS-PAGE) protein loading buffer (5×) (P0015L, Beyotime) or native-PAGE protein loading buffer (5×) (P0016, Beyotime), and heated at 100 °C for 5–10 min. Separation gels of various concentrations (6%, 7.5%, 10%, 12.5%, or 15%) were prepared as needed and underwent gel electrophoresis using a digital display voltage-stabilized current electrophoresis device (EPS-300, Tanon, Shanghai, China) set at 80–120 V for 60–100 min. Proteins were subsequently transferred onto a polyvinylidenefluoride (PVDF) membrane during an electrical transfer process set at 250–350 mA for 50–120 min. The membrane was blocked in 5% no-fat milk for 2 h, and incubated with the primary antibody at 4 °C for overnight on the shaker. On the next day, the primary antibody was washed off, and the secondary antibody was incubated with membrane at room temperature for 2 h. Finally, the immunoreactive bands were visualized using Tanon™ ECL chemiluminescence substrate (180-5001, Tanon) and analyzed and quantified using ImageJ software.

Omni-Easy™ One-step PAGE gel Rapid preparation kit was purchased from Epizyme (PG210, PG211, PG212, PG213, PG214, Shanghai Epizyme Biomedical Technology Co., Ltd., Shanghai, China), and 180 kDa Prestained ProteinMarker was purchased from Nanjing Vazyme (MP102-01/02, Vazyme, Nanjing, China) and 250 kDa from Epizyme (WJ103). Anti-ASC (CST-67824), glyceraldehyde phosphate dehydrogenase (GAPDH, 5174S), NLRP3 (CST-15101), nuclear factor-kappa B (p-NF-κB; 3033s), Jun N-terminal kinase (JNK; 9258s), LC3 1/2 (4108s), and SQSTM1/p62 (39749s) were purchased from Cell signaling Technology (Danvers, MA, USA). Anti- NF-κB inhibitor α (IκBα; bs3601), p-IκBα (bs4105), NF-κB (bs1257), p-JNK (bs4322), p38 (ap0424), p-p38 (bs4635), goat anti-rabbit lgG (H + L)-HRP (BS13278), goat anti-mouse lgG (H + L)-HRP (BS12478), and rabbit anti-goat lgG (H + L)-HRP (BS30503) were purchased from Bioworld. Anti-caspase-1 was purchased from Adipogen (AG-20B-0042, Adipogen, San Diego, CA, USA), anti-IL-1β was purchased from R&D (AB-401-NA, R&D, Minneapolis, MN, USA), and anti-GSDMD/GSDMD-NT was purchased from Abcam (ab219800, ab209845, Abcam, Cambridge, MA, USA).

2.10. Immunoprecipitation (IP) and CO-IP

2.10.1. Endogenous immunoprecipitation

BMDMs were pre-incubated with 200 ng/mL LPS for 3 h, followed by treatment with or without CQ for 1 h, and then stimulated with 10 mmol/L nigericin for 1.5–2.5 h. The cells were lysed in NP-

caspase-1, pro-IL-1β, gasdermin D (GSDMD) (GSDMD-NT) and apoptosis-associated speck-like protein containing a caspase activation and recruitment domain (CARD) (ASC) in lysates (LYS) of THP-1. LPS + nigericin (C), and LPS + MSU (F). (G) NLRP3-activated THP-1 cells were stained with propidium iodide (PI; red, dead cells) and 4′,6-diamidino-2-phenylindole (DAPI; blue, all cells) for 15–20 min, and then observed by fluorescence microscopy. (H) Quantification of dead cells by software ImageJ($n = 3$). (I) The representative images of the perforated scanning electron microscope created by GSDMD on the surface of THP-1 cells. Data are representative of n = 4 (A, C), $n = 3$ (B, E), and are expressed as mean ± standard deviation (SD). $^{*}P < 0.05$, $^{**}P < 0.01$, $^{***}P < 0.001$, ns: not significant, determined by Mann–Whitney test (A), Brown-Forsythe and Welch analysis of variance (ANOVA) tests (D) or one-way ANOVA with a Tukey test (B, D) (relative to LPS + nigericin/MSU). Glyceraldehyde phosphate dehydrogenase (GAPDH) served as a loading control in (C and F).

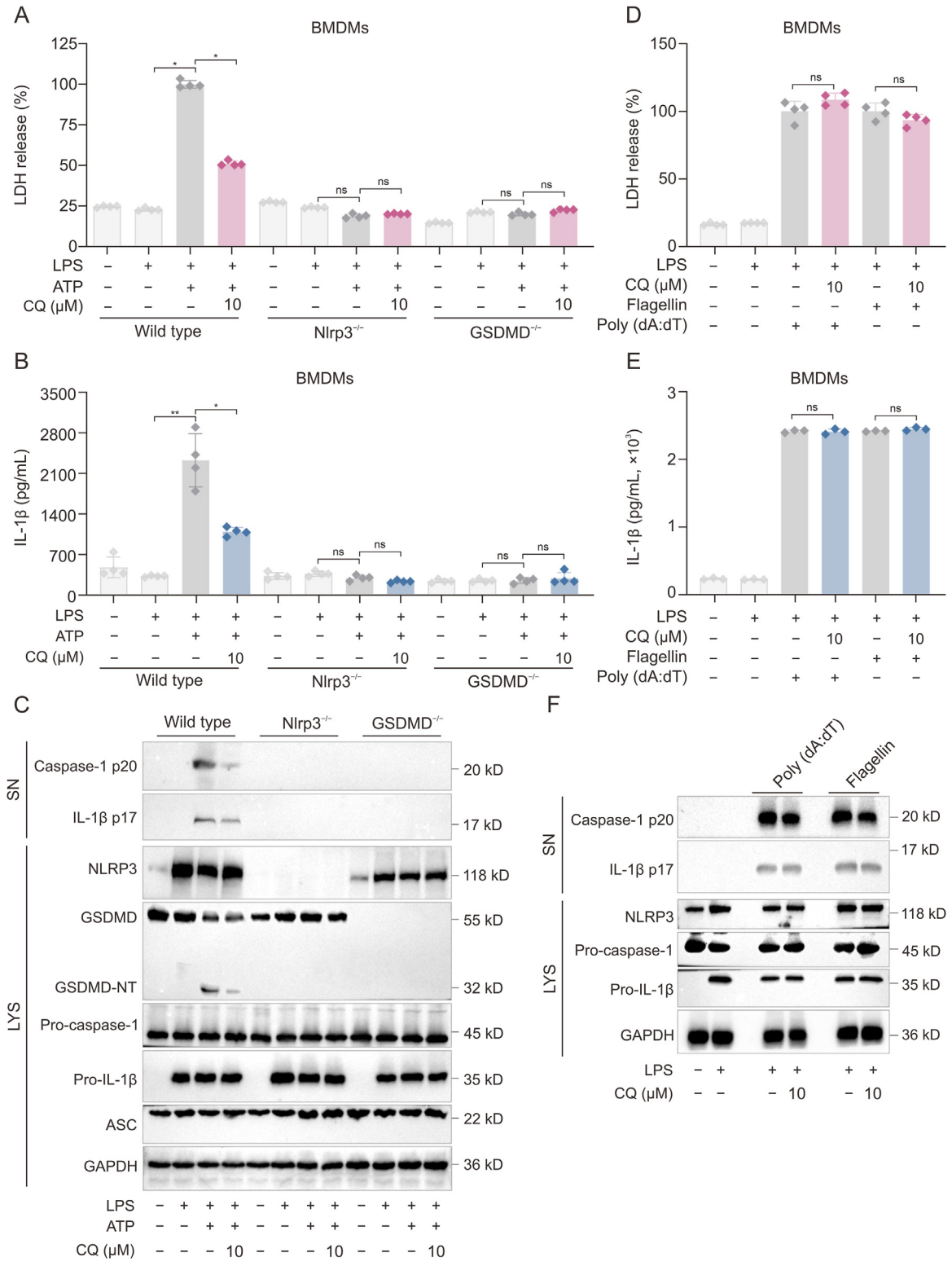

Fig. 3. Clioquinol (CQ) specifically inhibits the NOD-like receptor protein 3 (NLRP3) inflammasome activation. Lipopolysaccharide (LPS)-primed bone marrow-derived macrophage (BMDM) cells from wild type (WT), Nlrp3$^{-/-}$ and Gsdmd$^{-/-}$ mice were incubated with CQ for 1 h and then stimulated withATP for 0.5 h (A–C). LPS-primed BMDM cells were incubated with different doses of CQ for 1 h and then transfected with poly (dA: dT) or flagellin (D–F). (A, D) Lactate dehydrogenase (LDH) release in supernatant (SN) of cells. (B, E) Interleukin-1 beta (IL-1β) production in SN of cells was measured via enzyme-linked immunosorbent assay (ELISA). (C, F) Western blotting assay for IL-1β p17 and caspase-1 p20 levels in culture SN and NLRP3, pro-caspase-1, pro-IL-1β, gasdermin D (GSDMD) (GSDMD-NT) and apoptosis-associated speck-like protein containing a caspase activation and recruitment domain (CARD) (ASC) in lysates (LYS) of cells. Data are representative of $n = 4$ (A, B, D), $n = 3$ (C), and are expressed as mean ± standard deviation (SD). $^{*}P < 0.05$, $^{**}P < 0.01$, ns: not significant, determined by Mann–Whitney test (relative to LPS + nigericin) (A, B) or one-way analysis of variance (ANOVA) with a Tukey test (D, E) (relative to LPS + poly (dA: dT)/flagellin). Glyceraldehyde phosphate dehydrogenase (GAPDH) served as a loading control in (C, F). ATP: Adenosinetriphosphate.

40 lysis buffer containing 2% PMSF on ice for 30 min. Protein concentration was measured by the BCA Protein Assay Kit. Subsequently, 0.5 mL lysates together with 10 μL of resuspended volume of protein A/G plus-agarose were incubated at 4° C for 30 min. Pellet beads were centrifugated at 2,500 rpm for 5 min at 4° C, and supernatant (cell lysate) was transferred to a fresh 1.5 mL microcentrifuge tube on ice. After that, specific primary antibodies (2 μg) were added to the lysates and incubated for overnight at 4 °C in a shaker. On the next day, 20 μL of resuspended volume of protein A/G plus-agarose was added to the lysates, shaken at room temperature for 2 h, and centrifuged at 12,000 *g* for 10 min. The supernatant was removed, and the sediment was rinsed with pre-cooled 1× PBS. Afterward, the samples were resuspended in NP-40 lysate and protein loading buffer, heated at 100 °C for 10 min, and used for the subsequent western blotting.

2.10.2. CO-IP

HEK-293T cells were transfected with green fluorescent protein (GFP)-NLRP3, flag-(never in mitosis gene a)-related kinase 7 (NEK7), and flag-ASC plasmid overnight, and treated with CQ for 8 h. Cells were lysed with NP-40 lysis buffer (containing 2% PMSF) for 30 min, and quantified by BCA Protein Assay Kit. Anti-flag maganose beads (KTSM1338, AlpalifeBio, Shenzhen, China) were washed with 1× PBS for 3 times and then were added to prepared cell lysis, turning over on shaker for 2 h for full binding at 4 °C. The beads and supernatant were separated with magnetic-rack, and then washed beads with 1× PBS. The above steps were repeated for 4 times. The magnetic beads were then resuspended with 30 μL 1× SDS loading buffer (60 mM Tris-HCL (pH 6.8), 20% glycerol, 4% SDS, 0.04% bromophenol blue, 10% β-mercaptoehanol), heated at 100 °C for 10 min on metal bath, and used for the subsequent Western blotting.

2.11. Cross-linking of ASC oligomers

BMDMs were seeded to 6-well plates and incubated overnight at 37 °C in a 5% CO_2 incubator. After the mentioned treatments, cell lysates (lysed with NP-40) were centrifuged at 13,000 *g* for 20 min at 4 °C. Then, the pellets were washed twice with PBS. Then, 500 μL of disuccinimidyl suberate (S0657, Selleck) solution (2 mM) were added to the pellets and cross-linked for 60 min at room temperature on a shaker. After cross-linking, the pellets were resuspended in NP-40 lysis buffer containing SDS-PAGE sample loading buffer and boiled at 100 °C for 5–10 min for Western blot analysis.

2.12. NLRP3 oligomerization assay

The cells were pre-incubated with 200 ng/mL LPS for 3 h, and then treated with different concentrations of CQ for 1 h. Subsequently, the cells were stimulated with 10 mmol/L nigericin for 1.5 h to induce NLRP3 inflammasome. After treatments, cell lysates (lysed with NP-40) were centrifuged at 13,000 *g* for 20 min at 4 °C and then 1× native gel sample loading buffer was added after lysis and precast PAGE Gel (4%–20%, 10-well, abs9607, Absin, Shanghai, China) was used for native-PAGE Western blotting.

2.13. Detection of mitochondrial reactive oxygen species (ROS)

Following cell stimulation, cells were washed three times with pre-cold PBS and incubated in darkness with 5 μM MitoSOX Red Mitochondrial Superoxide Indicator (40778ES50, Yeasen, Shanghai, China) for 30 min. The cell membrane was permeabilized using a 0.05% Triton-X 100 solution and the nucleus was stained with a DAPI (5 μg/mL)solution for 10 min. Finally, cells were observed at a wavelength of 594 nm using a confocal laser microscope (FV3000, Olympus).

2.14. IL-1β/IL-6/tumor necrosis factor-α (TNF-α) cytokines enzyme-linked immunosorbent assay (ELISA)

The supernatants of cells, tissues, or serum collected in the previous experiment were utilized for cytokine determination. All ELISA assay kits (human IL-1β (CEK1731), mouse IL-1β (CEK1788), mouse IL-6 (CEK1785), mouse TNF-α (CEK1783)) were procured from Bioworld . The detailed protocol for the ELISA assay kit can be found in the reagent manufacturer's reference.

2.15. Drug affinity responsive target stability (DARTS)

The cells were pre-treated according to the previously mentioned inflammasome stimulation protocol, with one group receiving CQ and the other without. Cell lysis was performed as described earlier, followed by quantification of protein concentration in the lysate using a BCA protein quantification kit. The lysate was then divided into five equal aliquots. Pronase E (1.07433, Sigma-Aldrich) was added at concentrations of 0–10 μg/mL and incubated at room temperature for 20 min. The degradation reaction was stopped by adding 5–10 times more PMSF at 4 °C for 5–10 min. Samples of the completed reaction were mixed with protein sample buffer (5×), incubated in a metal bath at 100 °C for 5–10 min, and further analyzed through Western blotting.

2.16. Cellular thermal shift assay (CETSA)

The cells were pre-treated according to the previously mentioned inflammasome stimulation protocol. Specifically, they were divided into two groups: one group was treated with CQ and the other group was untreated. Protein concentration in the lysate was determined using a BCA protein quantification kit. Subsequently, the lysate was divided into six equal aliquots. To prevent cell damage and content leakage, trypsin digestion was performed on the treated cells, which was stopped by adding an equivalent volume of DMEM containing trypsin inhibitor. Cells were then centrifuged at 1,500 *g* for 5 min and washed with 1 mL of 1× PBS. After repeated centrifugation, 1× PBS was added and mixed with the cell pellet. The resulting cell suspension was evenly distributed into six portions and heated in a metal bath at temperatures ranging from 37 to 62 °C for 3 min each. Finally, rapid freeze-thaw cycles (3–5 times) using liquid nitrogen were applied to disrupt cellular structures before removing cell debris precipitates through centrifugation at 13,000 *g* for 10 min followed by appropriate addition of SDS-PAGE loading buffer (5×). Lastly, the samples underwent further analysis through protein immunoblotting.

2.17. NLRP3 ATPase activity assay

The HEK-293T cells were transfected with GFP-NLRP3 plasmid and pre-prepared. After replacing the medium, CQ was added for 40 min, followed by ultra-pure ATP at 37 °C for 30–60 min. Then, the conversion of ATP to ADP was quantified using the Promega GloMax 96 microplate luminescence detector. For detailed experimental procedures, please refer to the product manual of the ADP-Glo Kinase Assay Kit (S0150S, Beyotime). Three replicates were performed for each group.

2.18. Surface plasmon resonance (SPR)

SPR analysis was performed as previously described [15] to evaluate the interaction between CQ and the NACHT domain of human NLRP3 protein, using the BIAcore T200 instrument (BIAcore T200, GE Healthcare, Chicago, IL, USA). The human NLRP3 protein was initially purified and then immobilized on a CM5 sensor chip,

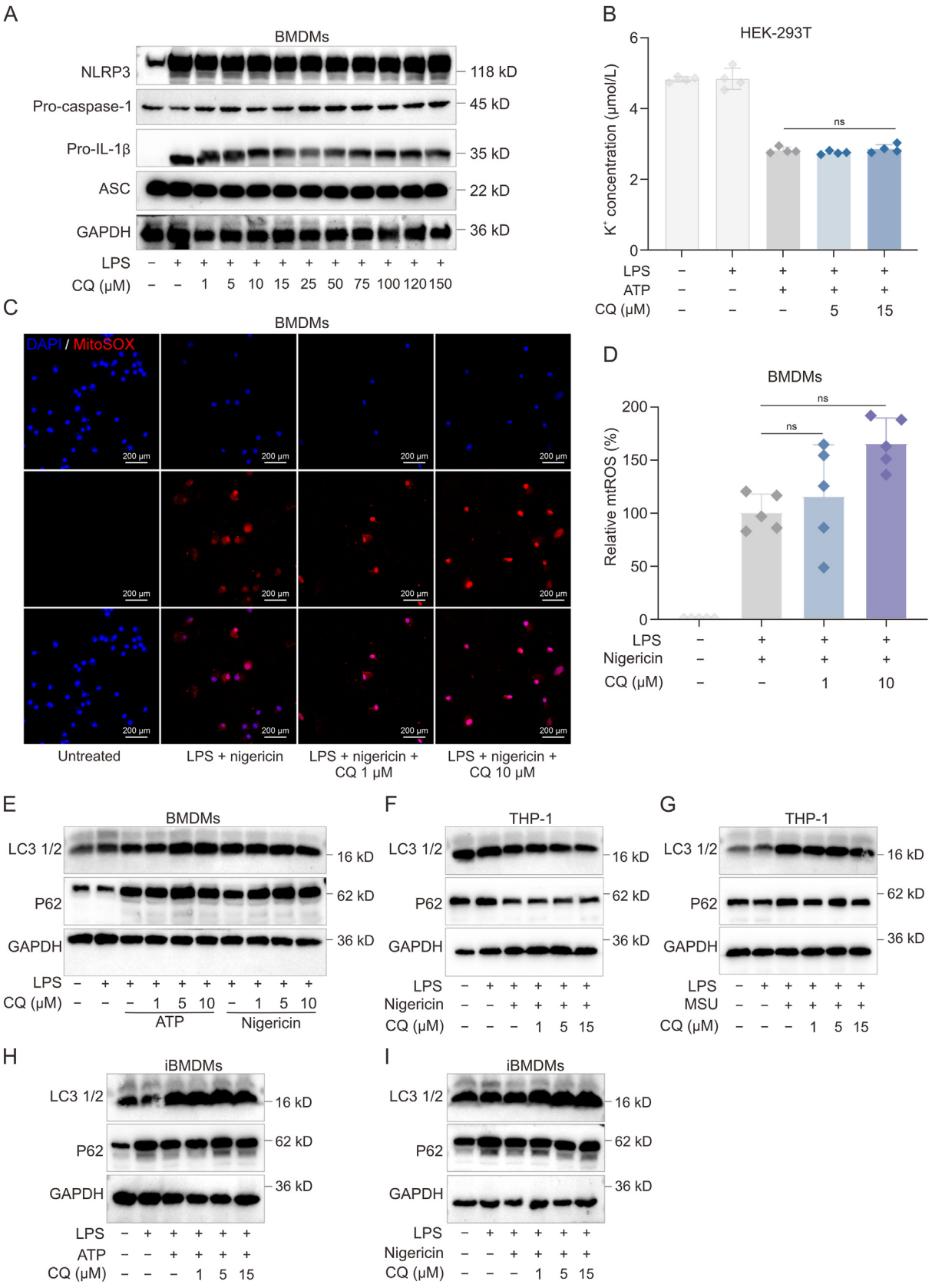

Fig. 4. Clioquinol (CQ) has no effect on NOD-like receptor protein 3 (NLRP3) upstream and cell autophagy. (A) bone marrow-derived macrophages (BMDMs) were pretreated with different doses of CQ for 2 h followed by stimulation with lipopolysaccharide (LPS) for 4 h. Western blot analysis of the protein expression of NLRP3, pro-caspase-1, pro-interleukin-1 beta (IL-1β) and apoptosis-associated speck-like protein containing a caspase activation and recruitment domain (CARD) (ASC). (B) LPS-primed BMDM cells were incubated with different doses of CQ for 40 min and then stimulated with ATP for 5–20 min, and K^+ concentrations in supernatants were measured by the potassium (K) turbidimetric assay kit. (C) LPS-primed BMDMs were treated with or without CQ for 1 h, and then were challenged with nigericin for 1 h. BMDMs were stained with MitoSOX, and then were observed using

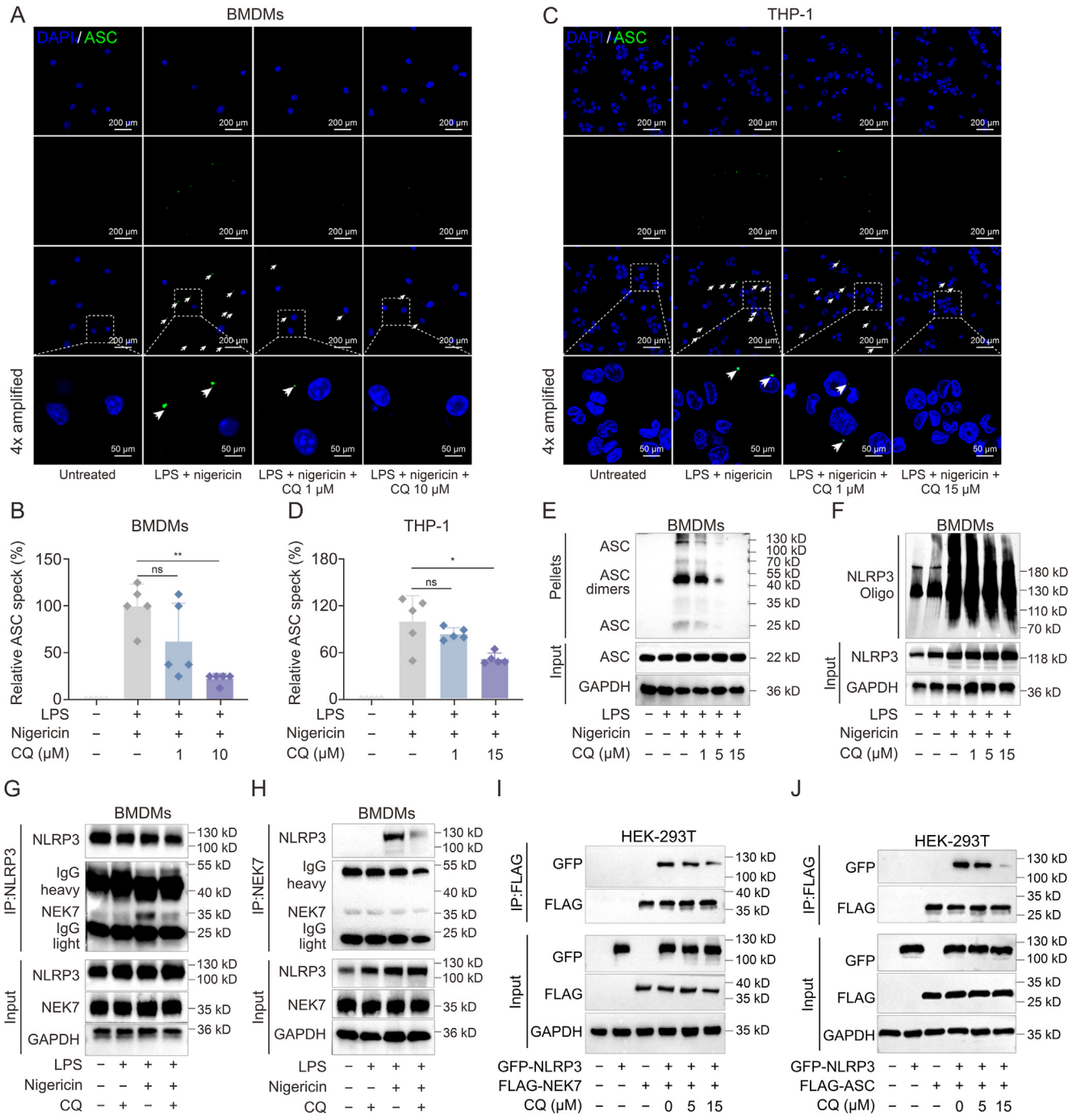

Fig. 5. Clioquinol (CQ) affects the interaction between NOD-like receptor protein 3 (NLRP3) and flag-(never in mitosis gene a)-related kinase (NEK)/apoptosis-associated speck-like protein containing a caspase activation and recruitment domain (CARD) (ASC). Lipopolysaccharide (LPS)-primed bone marrow-derived macrophages (BMDMs)/human monocyte leukemia cells (THP-1) cells were incubated with different doses of CQ for 1 h and then stimulated with nigericin for 1.5 h. (A, C) Immunofluorescence assay of ASC speck. BMDMs were stained with ASC antibody (green) and 4′,6-Diamidino-2-phenylindole (DAPI) (Blue). ASC speck formation was observed by immunofluorescence. BMDMs (A), and THP-1 cells (C). (B, D) The percentage of ASC specks was measured by ImageJ (relative to LPS + nigericin). BMDMs (B), and THP-1 cells (D). (E) Western blot analysis of ASC oligomerization level after cross-linking with disuccinimidyl suberate in NP-40-insoluble pellets from BMDMs. (F) NLRP3 self-oligomerization level was measured by native-polyacrylamide gel electrophoresis (PAGE). (G, H) Immunoprecipitation analysis of the interaction between NLRP3 and NEK7 in BMDMs. IP:NLRP3 (G), and IP:NEK7 (H). (I, J) Transfected HEK-293T with plasmid overnight and treated with CQ for 8 h, and then CO-immunoprecipitation (IP) with flag antibody and Western blot was used to evaluate the interaction between green fluorescent protein (GFP)-NLRP3 and FLAG-NEK7 (I) or FLAG-ASC (J). Data are representative of $n = 5$ (B, D), and are expressed as mean ± standard deviation (SD). $^{*}P < 0.05$, $^{**}P < 0.01$, ns: not significant, determined by Mann–Whitney test (relative to LPS + nigericin). Glyceraldehyde phosphate dehydrogenase (GAPDH) served as a loading control in (E–G).

fluorescence microscope. The representative graphics are shown (Red: MitoSOX; Blue: 4′,6-Diamidino-2-phenylindole (DAPI), showing nuclei). (D) by ImageJ ($n = 5$). (E–I) LPS-primed cells were treated with or without CQ for 1 h, and then were challenged with adenosinetriphosphate (ATP) or nigericin. Western blot analysis of the protein expression of LC3 1/2 and P62. BMDMs (E), human monocyte leukemia cells (THP-1) (F, G) and immortalized bone marrow-derived macrophages (iBMDMs) (H, I). Data are representative of $n = 4$ (B), $n = 5$ (D), and are expressed as mean ± standard deviation (SD). ns: not significant, determined by one-way analysis of variance (ANOVA) with a Tukey test (B) (relative to LPS + ATP) (A, B) or Kruskal–Wallis test (D) (relative to LPS + nigericin). Glyceraldehyde phosphate dehydrogenase (GAPDH) served as a loading control in (A, E–I).MSU: monosodium urate.

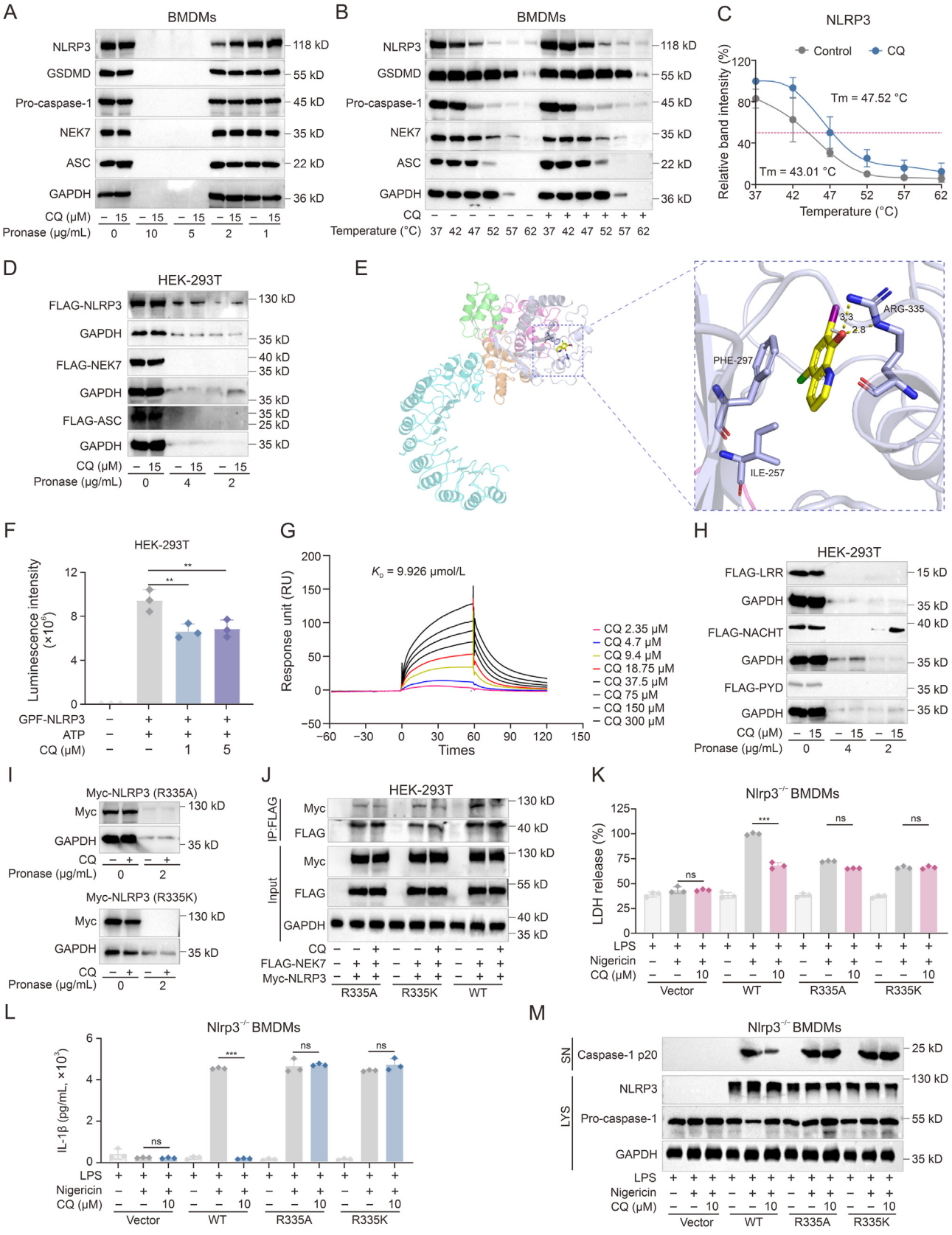

Fig. 6. Clioquinol (CQ) inhibits NOD-like receptor protein 3 (NLRP3) activation by targeting arginine 335 (ARG335) of NACHT. (A) Drug affinity responsive target stability (DARTS) assay was performed with pronase E (0–10 μg/mL) in the presence or absence of CQ (15 μM). (B) The thermal stability of NLRP3, gasdermin D (GSDMD) , pro-caspase-1 and ASC protein in BMDMs treated with or without CQ was measured by cellular thermal shift assay (CETSA). NLRP3, GSDMD, pro-caspase-1 and apoptosis-associated speck-like protein containing a caspase activation and recruitment domain (CARD) (ASC) protein levels were analyzed by Western blotting. (C) The relative band intensity of NLRP3 in (B) was calculated by ImageJ software (normalization with glyceraldehyde phosphate dehydrogenase (GAPDH)). (D) Transfected HEK-293T cells with high-expression FLAG-NLRP3, FLAG-

with a blank channel serving as the negative control. Subsequently, CQ underwent serial dilution with PBS buffer and was passed through the chip. All solutions were meticulously prepared using ultrapure water and filtered through a 0.22 μm membrane filter. The experiments conducted on the BIAcore T200 were carefully maintained at 25 ± 1 °C, with the BIAcore T200 flowing system being primed with a running buffer before each analysis. The K_D value was determined utilizing a steady affinity state model via the BIAcore T200 analysis software.

2.19. Experimental molecular docking

The molecular docking experiment was performed as previously described [16]. Utilized the NLRP3 ID: 6NPY retrieved from the Protein Data Bank (PDB) database. Initially, protein crystallization water and original ligands were removed using Pymol 2.3.0. Subsequently, the protein structure underwent hydrogenation, charge calculation, charge assignment, and atom type specification using AutoDocktools (v1.5.6). The docking procedure was conducted employing AutoDock Vina 1.1.2. Parameters pertinent to NLRP3 were set as follows: center_x = 87.015, center_y = 95.575, center_z = 91.600; search space dimensions were defined as size_x: 60, size_y: 60, size_z: 60 (with a grid spacing of 0.375 Å per grid point); exhaustiveness was set to 10, while the remaining parameters were maintained at default values. Following the docking simulations, the resultant interaction patterns were analyzed using PyMOL 2.3.0.

2.20. K^+ concentration assay

The inflammasome was activated in the same manner as previously mentioned, and subsequently, cell supernatant was collected for determination of potassium concentration using the Potassium (K) turbidimetric Assay Kit (E-BC-K279-M, Elabscience, Wuhan, China). The methodology is outlined in the manufacturer's manual.

2.21. Virus-mediated overexpression

BMDMs were prepared and infected at a multiplicity of infection (MOI) of 30–50 with lentivirus-overexpression, which were prepared by Nanjing Corues Biotechnology. The lentivirus-overexpression (R335A and R335K) was used for the infection. BMDMs were separately infected with lentivirus or adenovirus for 72 h before further treatments.

2.22. Hematoxylin and eosin (H&E) staining

The histological changes were examined with H&E stain as previously described [17]. Briefly, the mice were euthanized and perfused with 1× PBS and 4% PFA. The liver, kidney, lung, foot joint, and intestine tissues were collected and post-fixed in 4% PFA for overnight, and transported to Wuhan Service Biotechnology Co., Ltd. (Wuhan, China) for H&E staining. Detailed methods are described as follows: Paraffin sections were dewaxed using environmentally friendly dewaxing transparent liquid I and II (D292661, Aladdin, Shanghai, China), followed by anhydrous ethanol I and II, and 75% ethyl alcohol (64-17-5, Xilong Scientific, Shanghai, China). The sections were then rinsed with tap water. Frozen sections were brought to room temperature, fixed with the tissue-fixing solution for 15 min, and rinsed with running water. H&E Staining Kit was purchased from Abcam (ab245880), then treated with HD constant staining pretreatment solution for 1 min and stained with hematoxylin solution for 3–5 min, followed by treatment with hematoxylin differentiation solution for 3–5 min, and then stained with hematoxylin bluing solution for 1 min.After that, the sections were stained in 95% ethanol followed by eosin dye. Sections underwent dehydration using absolute ethanol I–III, normal butanol I–II (71-36-3, Xilong Scientific), xylene I and xylene II (1330-20-7, Xilong Scientific) before being sealed using neutral gum.

2.23. Colonial histology score

The colon tissues were fixed in 4% PFA at room temperature and subsequently subjected to H&E staining as methods described above. The histological assessment of the H&E-stained colonic sections was graded as follows: 0, no inflammation; 1, minimal leukocyte infiltration; 2, moderate leukocyte infiltration; 3, significant leukocyte infiltration, moderate fibrosis, increased vascular density, thickening of the colon wall, moderate loss of goblet cells, and focal crypt loss; 4, transmural infiltrations, extensive goblet cell loss, pronounced fibrosis, and diffuse crypt loss.

2.24. Caspase-1 activity assay

After euthanizing the arthritis model mice, foot pad tissues were collected and incubated in serum-free DMEM medium for 1 h. The supernatant was then obtained by centrifugation and used for determining caspase-1 activity using the Caspase-1 Activity Assay Kit (C1102, Beyotime). The determination procedure followed the manufacturer's instructions.

2.25. Mice model of gouty arthritis induced by MSU

Male C57BL/6 mice, aged 8–10 weeks, were pretreated with CQ (i.p) one day prior to the experiment. After an interval of 8–12 h, a second dose of CQ was administered. Subsequently, MSU crystals at a dose of 0.6 mg were injected into the left foot joint after 1 h while no solution was injected into the right foot as a control. The thickness of the foot joint was measured hourly using a vernier caliper and the difference in thickness between the left and right feet was used to evaluate arthritis severity. Additionally, continuous monitoring of footpad thickness was conducted for 6 h. Following this period, mice were euthanized and perfused with PBS and 4% PFA. Mouse foot joints were then collected for assessment of caspase-1 activity, IL-1β ELISA analysis, and H&E staining.

(never in mitosis gene a)-related kinase 7 (NEK7) and FLAG-ASC plasmids for 36 h, and collected cell LYS to incubate CQ overnight followed by DARTS assay. (E) The hydrogen bonds formed between CQ and NLRP3 by molecular docking. (F) HEK-293T cells transfected with green fluorescent protein (GFP)-NLRP3 plasmid and then treated with CQ. The luminescence intensity was detected by ADP-Glo Kinase Assay Kit. (G) A kinetic analysis was conducted to investigate the direct interaction between CQ and immobilized recombinant human NLRP3 protein, utilizing the single-cycle surface plasmon resonance (SPR) technique. (H) DARTS assay of LRR, NACHT and PYD in the presence or absence of CQ in HEK-293T cells transfected with FLAG-LRR, FLAG-NACHT and FLAG-PYD plasmids for 36 h. (I) DARTS assay of mutant Myc-NLRP3 (R335A/R335K) in the presence or absence of CQ in HEK-293T cells. (J) Immunoprecipitation (IP) and Western blot analysis were performed to assess the interaction between NEK7 and wild type (WT) or mutant NLRP3 (R335A/R335K) in HEK-293T cells treated with or without CQ. (K–M) LPS-primed Nlrp3$^{-/-}$ BMDMs reconstituted with WT or mutant NLRP3 (R337A, R337K) were pretreated with CQ and then stimulated with nigericin. Lactate dehydrogenase (LDH) release in supernatant (SN) of cells (K). The levels of interleukin-1 beta (IL-1β) in SN were measured by enzyme-linked immunosorbent assay (ELISA) (L). The protein levels of caspase-1 p20 in cell SN, and NLRP3, pro-caspase-1 in cell LYS were detected by Western blot (M). Data are representative of $n = 3$ (C, F, K, L), and are expressed as mean ± standard deviation (SD). $^{**}P < 0.01$, $^{***}P < 0.001$, ns: not significant, determined by one-way analysis of variance (ANOVA) test (relative to LPS + ATP/nigericin). Glyceraldehyde phosphate dehydrogenase (GAPDH) served as a loading control in (A, B, D, H–J, M). Vector: lentivirus that contains empty plasmids (no target gene).

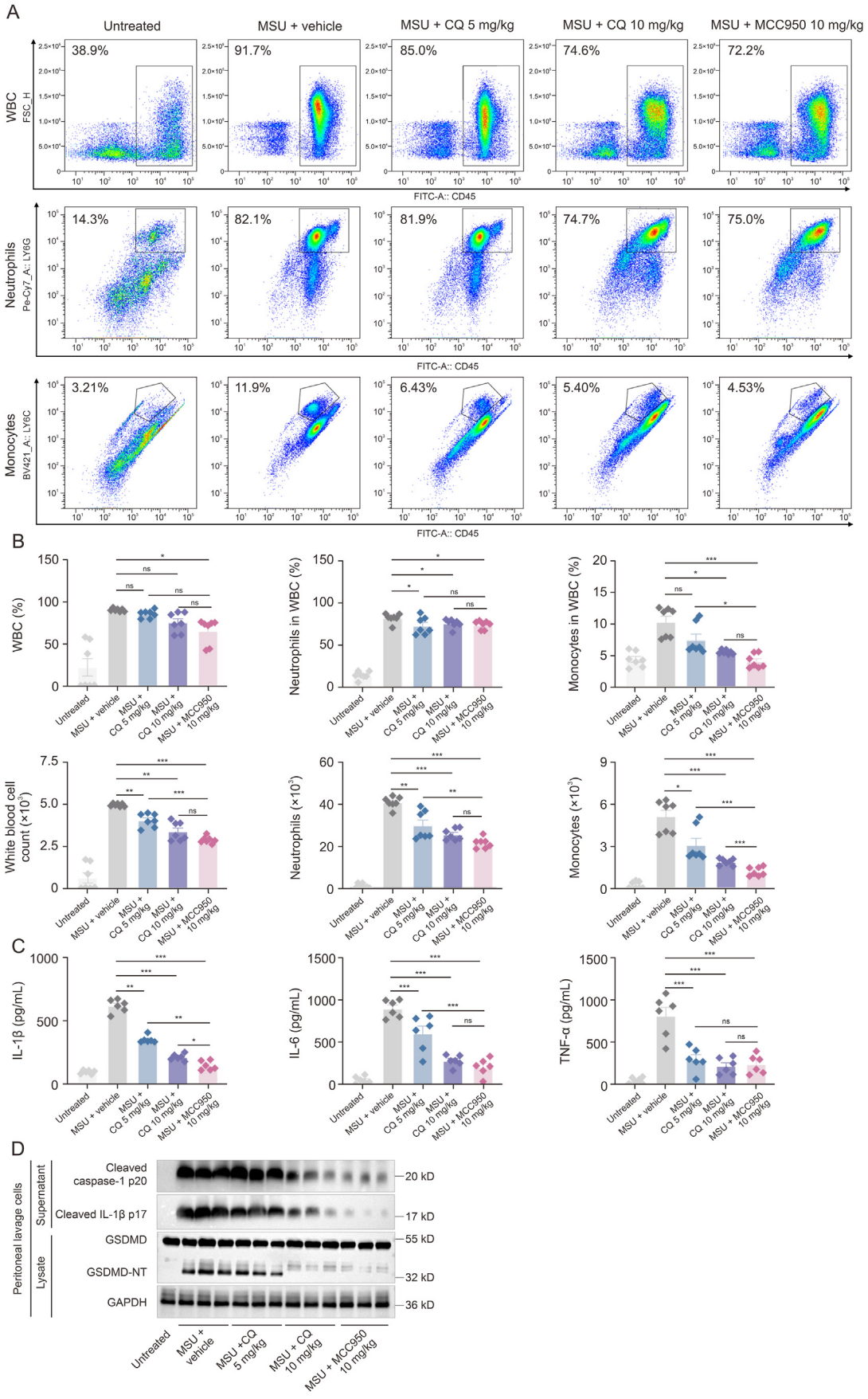
A
Untreated
MSU + vehicle
MSU + CQ 5 mg/kg
MSU + CQ 10 mg/kg
MSU + MCC950 10 mg/kg
WBC
FSC_H
38.9%
91.7%
85.0%
74.6%
72.2%
FITC-A:: CD45
Neutrophils
Pe-Cy7_A:: LY6G
14.3%
82.1%
81.9%
74.7%
75.0%
FITC-A:: CD45
Monocytes
BV421_A:: LY6C
3.21%
11.9%
6.43%
5.40%
4.53%
FITC-A:: CD45
B
WBC (%)
Neutrophils in WBC (%)
Monocytes in WBC (%)
White blood cell count (×10³)
Neutrophils (×10³)
Monocytes (×10³)
C
IL-1β (pg/mL)
IL-6 (pg/mL)
TNF-α (pg/mL)
D
Peritoneal lavage cells
Supernatant
Lysate
Cleaved caspase-1 p20
Cleaved IL-1β p17
GSDMD
GSDMD-NT
GAPDH
20 kD
17 kD
55 kD
32 kD
36 kD
Untreated
MSU + vehicle
MSU + CQ 5 mg/kg
MSU + CQ 10 mg/kg
MSU + MCC950 10 mg/kg

2.26. Mice model of peritonitis induced by MSU

The C57BL/6 mice, aged 8–10 weeks, received repeated injections of CQ every 8–12 h. After 1 h, each mouse was intraperitoneally injected with 0.8 mg MSU. 6 h later, the peritoneal cavity was washed with pre-cooled 1× PBS solution containing 0.5 mM ethylene diamine tetraacetic acid (EDTA; 1852916, Invitrogen, Carlsbad, CA, USA) and collected for centrifugation at a temperature of 4 °C and a speed of 1,500 *g*. The cells were used for flow cytometry analysis while the supernatant was utilized for IL-1β and IL-6 ELISA assays.

2.27. Mice model of sepsis induced by LPS

Male C57BL/6 mice, aged 8–10 weeks, were pre-injected intraperitoneally with CQ 1 day prior to receiving repeated injections of CQ at an interval of 8–12 h. After 1 h, each mouse was injected (i.p) with a solution containing 0.3 mg LPS. At the peak of inflammation after 12 h, orbital blood samples were collected for subsequent analysis. Flow cytometry was performed using peripheral blood samples, while serum samples were used for IL-1β, IL-6, and TNF-α ELISA assays. Subsequently, mice were perfused with PBS followed by fixation with 4% PFA, and lungs and livers were harvested for H&E staining.

2.28. Mice model of UC induced by DSS

Male C57BL/6 mice, aged 8–10 weeks, were grouped as previously described, with seven mice per group. A 4% DSS solution was prepared by dissolving DSS in sterile water and provided to the mice through their drinking water dispenser. After 8 day of treatment, normal drinking water was reinstated and the mice were fed for an additional 3 day. Medication administration was started on the day of modeling and involved daily intraperitoneal injections while body weight, stool consistency, and fecal blood presence were monitored.

The disease activity index (DAI) scoring criteria were defined as follows: Body weight loss (0–5): 0, none; 1, 1%–5%; 2, 6%–10%; 3, 11%–15%; 4, 16%–20%; and 5, >20%. Stool consistency (0–4): 0, normal; 1, soft but still formed; 2, very soft; 3, very soft and moist; and 4, watery diarrhea. Fecal blood (0–4): 0-negative for blood; 1-faintly positive for blood; 2-positive for blood; 3-visible blood in feces; and 4-rectal bleeding.

Euthanasia of the mice was performed on the 7 day, followed by collection of serum and colon samples for ELISA analysis.

2.29. Flow cytometry

Animal model cell suspensions were washed with pre-cooled 1× PBS using different methods and lysed with red cell lysis buffer 1–3 times if red blood cells were present. Antibodies, including anti-CD11B (53-0112-82, eBioscience, San Diego, CA, USA), anti-CD45 (25-0451-82, eBioscience), anti-CD4 (17-0042-82, eBioscience), anti-CD8 (11-0081-85, eBioscience), anti-F4/80 (BM8, Biolegend, San Diego, CA, USA), anti-LY6C (HK1.4, Biolegend) and anti-LY6G (12-5931-81, eBioscience) at respective ratios of 1:500–1:1000 were mixed and added to the cell suspension in an Eppendorf (EP) tube for staining at 4 °C for 30 min in darkness. After centrifugation at a speed of 800 *g* for 5 min and washing with PBS 1–3 times, the cells were resuspended in an appropriate proportion of PBS and analyzed by BD Fortessa flow cytometry (BD Biosciences, San Jose, CA, USA). Data was analyzed using FlowJo_v10.6.2 software.

2.30. Statistical analysis

The data was analyzed using GraphPad Prism 8.0 software, and the results are presented as mean ± standard deviation (SD) S1–2 or mean ± standard error of the mean (SEM)S3–4. Statistical analysis was determined using analysis of variance (ANOVA) for multiple comparisons. Additionally, One-way ANOVA, Mann–Whitney test, or unpaired Student's *t*-test was used for multiple-group analyses ($^{*}P < 0.05$, $^{**}P < 0.01$, $^{***}P < 0.001$) by GraphPad Software. It should be noted that all data were obtained from a minimum of 3 independent experiments.

3. Results

3.1. CQ effectively suppressed NLRP3-mediated pyroptosis in both mouse and human macrophages

Before initiating cell experiments, the cytotoxicity of CQ on three cell types—BMDMs, THP-1 cells, and iBMDMs—was validated using the CCK8 assay (Fig. S1). Non-cytotoxic concentrations were selected for subsequent experiments. To evaluate CQ's impact on NLRP3 inflammasome activation, BMDMs, THP-1 cells, and iBMDMs were pretreated with CQ or vehicle and then activated with NLRP3 inflammasome activators (ATP, nigericin, or MSU) in LPS-primed cells. CQ significantly reduced LDH release in BMDMs (Fig. 1A) and effectively inhibited IL-1β secretion (cleaved by caspase-1) in cell culture supernatants, a hallmark of NLRP3 inflammation activation (Fig. 1B). Immunoblotting analysis revealed that CQ inhibits the release of cleaved caspase-1 p20 and IL-1β p17 fragments into the extracellular space while not affecting the expression levels of NLRP3, pro-Caspase-1, pro-IL-1β, and ASC within cellular lysates (Fig. 1C).

Dual fluorescence staining with DAPI, a fluorescent dye employed for viable cell labelling, and PI, which stains non-viable cells, enabled the simultaneous analysis of live and dead cell populations. CQ dose-dependently reduced the proportion of PI-positive BMDMs following nigericin stimulation (Fig. 1D). Quantitative fluorescence analysis confirmed that CQ significantly decreases the number of dead cells (Fig. 1E). CQ demonstrated an IC_{50} value of 0.478 μM against LPS- and nigericin-induced pyroptosis in BMDMs, compared to the NLRP3 classic inhibitor MCC950 (IC_{50} = 0.275 μM) (Fig. 1F). Corresponding studies on human macrophages THP-1 cells revealed that CQ similarly inhibits NLRP3 inflammasome activation and pyroptosis (Figs. 2A–F). CQ effectively reduces cell death in LPS-primed THP-1 cells, as evidenced by DAPI and PI staining (Figs. 2G and H). Scanning electron microscopy showed that membrane perforation caused by GSDMD-NT on the surface of THP-1 cells was significantly reduced in CQ-treated cells (Fig. 2I). Similar results were observed in iBMDMs (Fig. S2). Pro-caspase-1 (p45)/active caspase-1 (p20) and IL-1β precursor/

Fig. 7. Clioquinol (CQ) suppresses monosodium urate (MSU)-induced acute peritonitis effectively. (A) White blood cell (WBC; CD 45^{+}), neutrophils (CD $11B^{+}$ $Ly6G^{+}$) and monocytes (CD $11B^{+}$ $Ly6C^{+}$) in the peritoneum of mice were detected by flow cytometry. Numbers in plots indicate percentage of cells. (B) Flow cytometry analysis of WBC, neutrophils, monocytes percentage and numbers in the peritoneal cavity of mice injected with MSU with or without CQ (i.p.). (C) Interleukin (IL)-1β), IL-6 and tumor necrosis factor-α (TNF-α) production in peritoneal lavage fluid was assessed by enzyme-linked immunosorbent assay (ELISA). (D) NOD-like receptor protein 3 (NLRP3)-related protein expression in peritoneal lavage cells. Data are representative of $n = 7$, and are expressed as mean ± standard error of the mean (SEM). $^{*}P < 0.05$, $^{**}P < 0.01$, $^{***}P < 0.001$, ns: not significant, determined by analysis of variance (ANOVA) or Mann–Whitney test (relative to MSU + dimethyl sulfoxide (DMSO)). Glyceraldehyde phosphate dehydrogenase (GAPDH) served as a loading control in (D). GSDMD: gasdermin D.

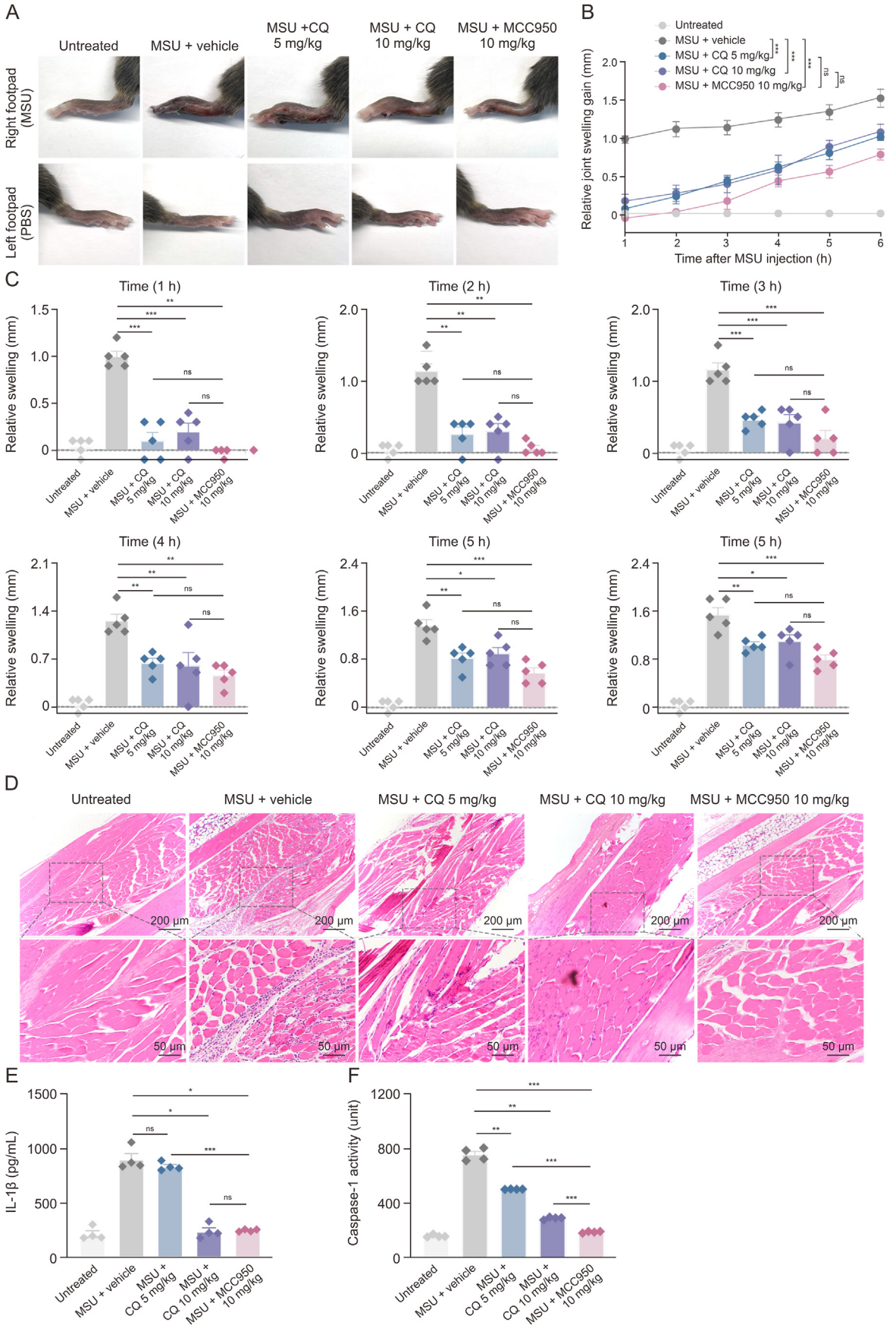
A
Untreated
MSU + vehicle
MSU +CQ 5 mg/kg
MSU + CQ 10 mg/kg
MSU + MCC950 10 mg/kg
Right footpad (MSU)
Left footpad (PBS)
B
Untreated
MSU + vehicle
MSU + CQ 5 mg/kg
MSU + CQ 10 mg/kg
MSU + MCC950 10 mg/kg
Relative joint swelling gain (mm)
Time after MSU injection (h)
C
Time (1 h)
Time (2 h)
Time (3 h)
Time (4 h)
Time (5 h)
Time (5 h)
Relative swelling (mm)
D
200 μm
50 μm
E
IL-1β (pg/mL)
F
Caspase-1 activity (unit)

mature IL-1β levels were detected both in supernatant and lysate (Fig. S3). In conclusion, CQ possesses significant anti-pyroptosis properties.

3.2. CQ specifically inhibits the activation of NLRP3 inflammasome

To further assess CQ's specificity in inhibiting the NLRP3 inflammasome, primary BMDMs were isolated from 8-week-old NLRP3-deficient and GSDMD-deficient mice for *in vitro* experiments. The absence of NLRP3 resulted in the inhibition of inflammasome activation, cleavage of the downstream pyroptosis-executing molecule GSDMD, and the release of inflammatory factors. In NLRP3 and GSDMD knockout cells, CQ failed to inhibit the cleavage of IL-1β, caspase-1, and GSDMD (Figs. 3A and B). Western blot analysis confirmed the absence of GSDMD-NT, caspase-1 p20, and IL-1β p17, indicating no occurrence of pyroptosis (Fig. 3C). The AIM2 inflammasome, a cytoplasmic protein complex detecting DNA and triggering inflammation, and the NLRC4 inflammasome, composed of the NLR family protein NLRC4 that regulates inflammatory and immune responses, were also studied. Transfection of BMDM cells with Poly (dA: dT) and flagellin activated the AIM2 and NLRC4 inflammasomes, respectively (Figs. 3D–F). Results demonstrated that CQ had no significant effects on flagellin/NLRC4 and poly (dA: dT)/AIM2-mediated pyroptosis (Figs. 3D–F).

These results suggest that CQ lacks inhibitory effects on other inflammasome activations, highlighting its potential role as a specific inhibitor of NLRP3 inflammasome activation.

3.3. CQ does not impact the upstream events of NLRP3 activation

To further elucidate the mechanism by which CQ inhibits NLRP3 activation, Western blotting was utilized to analyze the core components of the NLRP3 inflammasome, including NLRP3, pro-caspase-1, pro-IL-1β, and ASC proteins. Results showed that these proteins remained unchanged after CQ treatment in macrophages (Fig. 4A), suggesting that CQ reduces inflammation and pyroptosis regardless of the initial signalling events involved in NLRP3 inflammasome activation.

Furthermore, the potential impact of CQ on ATP-induced potassium efflux was investigated, revealing that K^+ efflux was unaffected by CQ treatment (Fig. 4B). Mitochondrial dysfunction, generation of mitochondrial reactive oxygen species (mtROS), and release of mitochondrial DNA (mtDNA) into the cytoplasm are critical upstream events implicated in NLRP3 activation. Under stress conditions, mitochondria continuously release reactive oxygen species as byproducts of oxidative phosphorylation, substantially increasing mtROS levels (Figs. 4C and D). The findings indicated that CQ did not influence mitochondrial damage. Additionally, the role of autophagy in CQ's mechanism was examined by evaluating the expression levels of intracellular LC3 1/2 and P62 proteins. Results demonstrated that CQ does not affect their expression, indicating that the inhibitory effect on NLRP3 inflammasome activation and cell pyroptosis is not mediated through modulation of the autophagy pathway (Figs. 4E–I).

These results imply that CQ does not interfere with upstream events associated with NLRP3 activation nor specifically induce autophagy activation.

3.4. CQ inhibits the assembly of NLRP3 inflammasomes

NLRP3 operates as a receptor protein, detecting cellular damage and pathogen invasion, thereby initiating inflammatory responses. NEK7, a kinase protein, interacts with NLRP3 to regulate its activity. ASC oligomerization is essential for assembling the NLRP3 inflammasome, an essential step in subsequent caspase-1 activation [18]. This intricate interplay among NLRP3, NEK7, and ASC regulates inflammatory responses. To investigate CQ's impact on the interaction between NLRP3 and ASC, immunofluorescence assays were employed to examine the effect of CQ on ASC specks in BMDMs. CQ treatment attenuated the fluorescence signals representing ASC specks, indicating that CQ suppressed nigericin-induced ASC oligomerization in both BMDMs (Figs. 5A and B) and THP-1 cells (Figs. 5C and D). These results suggest that CQ inhibits NLRP3 inflammasome activation by suppressing the assembly of inflammasome components. Specifically, CQ inhibits the formation of ASC oligomers (Fig. 5E). Upon stimulation, self-oligomerization of NLRP3 leads to its binding with ASC protein, forming the "NLRP3-ASC-Caspase-1" [19] complex, which triggers inflammasome assembly and promotes inflammation. CQ impedes this self-oligomerization mechanism within NLRP3 itself (Fig. 5F), suggesting an ATPase-dependent inhibition of NLRP3 oligomerization. Immunoprecipitation experiments confirmed the effective disruption of endogenous interactions between NLRP3-NEK7 (Fig. 5G) and NLRP3-ASC (Fig. 5H) following CQ treatment. To further validate these findings, tagged plasmids encoding the respective components were generated and transfected into HEK-293T cells for co-immunoprecipitation analysis. Consistently, CQ impeded the interaction between NLRP3-NEK7 (Fig. 5I) and NLRP3-ASC (Fig. 5J) in plasmid-transfected HEK-293T cells.

3.5. CQ directly binds to NLRP3 at ARG335 of NLRP3

Next, the investigation focused on whether CQ inhibits NLRP3 activation by directly binding to NEK7 or ASC, or by interacting with NLRP3 itself. Two established techniques, CETSA and DARTS, were employed to assess drug-target protein interactions within cellular contexts. CETSA measures binding affinity through the stabilization of protein conformation, while DARTS confers resistance against proteolytic cleavage via drug–protein interactions [20]. In the DARTS assay, pre-incubation of CQ with BMDM cell lysates attenuated pronase-induced proteolysis of NLRP3, but did not affect GSDMD, NEK7, ASC, or caspase-1 proteins (Fig. 6A). This suggests that CQ may specifically interact with NLRP3. In the CETSA assay, BMDMs pre-treated with CQ exhibited significantly higher thermal stability compared to the control group under identical temperature conditions (Fig. 6B). Quantitative analysis provided further insights into the protective effect of CQ on NLRP3 (Fig. 6C). The thermal melting curve from the CQ-treated group displayed a significant rightward shift compared to the control group. These results from both CETSA and DARTS assays suggest a direct interaction between CQ and NLRP3, warranting further investigation.

To confirm these results, experiments were conducted in plasmid-transfected HEK-293T cells. As expected, CQ increased the thermal stability of NLRP3 (Fig. 6D). Molecular docking simulations identified potential binding regions between NLRP3 and CQ, with a

Fig. 8. Clioquinol (CQ) significantly improves monosodium urate (MSU)-induced gouty arthritis. 8–10 weeks C57BL/6 male mice were pre-injected with or without CQ/MCC950 (i.p) twice, and then injected with MSU into footpad for 6 h. (A) The representative photos of mice footpads, MSU (right footpad), PBS (left footpad). (B, C) The footpad thicknesses were measured by vernier caliper during 6 h. (D) Representative hematoxylin and eosin (H&E) staining of mice footpads. (E) Interleukin-1 beta (IL-1β) levels in the joint culture supernatant (SN). (F) Activity of caspase-1 in the joint culture SN. Data are representative of $n = 5$ (B, C), $n = 4$ (E, F), and are expressed as mean ± standard error of the mean (SEM). $^{*}P < 0.05$, $^{**}P < 0.01$, $^{***}P < 0.001$, ns: not significant, determined by analysis of variance (ANOVA) or Mann–Whitney test (relative to MSU + dimethyl sulfoxide (DMSO)).

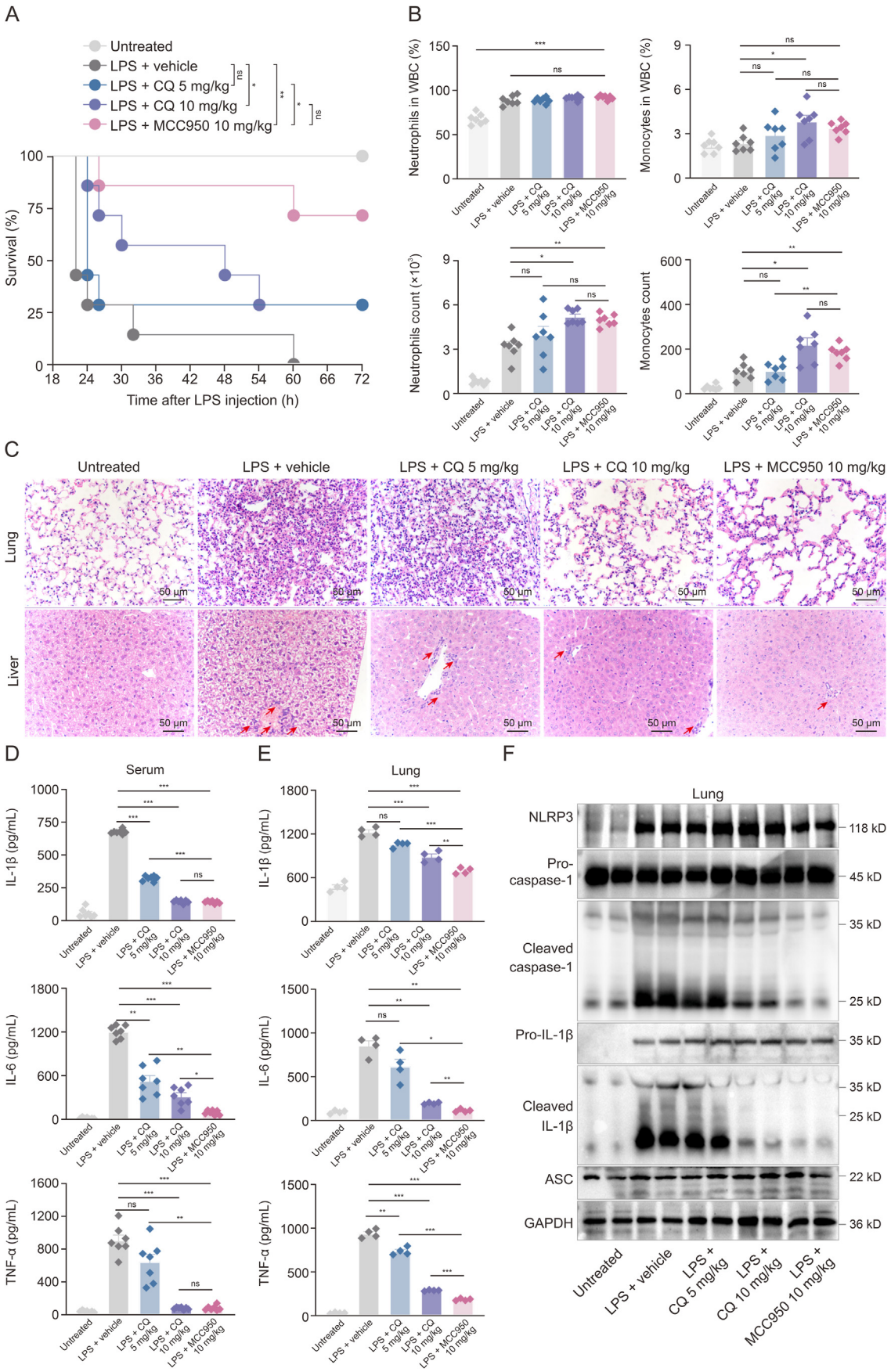
A
Untreated
LPS + vehicle
LPS + CQ 5 mg/kg
LPS + CQ 10 mg/kg
LPS + MCC950 10 mg/kg
Survival (%)
Time after LPS injection (h)
B
Neutrophils in WBC (%)
Monocytes in WBC (%)
Neutrophils count (×10³)
Monocytes count
C
Lung
Liver
50 μm
D
Serum
IL-1β (pg/mL)
IL-6 (pg/mL)
TNF-α (pg/mL)
E
Lung
F
Lung
NLRP3
Pro-caspase-1
Cleaved caspase-1
Pro-IL-1β
Cleaved IL-1β
ASC
GAPDH
118 kD
45 kD
35 kD
25 kD
35 kD
35 kD
25 kD
22 kD
36 kD

binding energy of −6.5 kcal/mol (Fig. 6E). Hydrogen bonding interactions and hydrophobic forces primarily contributed to the association, with CQ establishing hydrogen bonds with ARG-335, measuring 3.3 Å and 2.8 Å, respectively. The ATPase activity of GFP-NLRP3 in transfected HEK-293T cells was assessed with and without CQ treatment, revealing a dose-dependent suppression of GFP-NLRP3 ATPase activity by CQ (Fig. 6F). To further validate these results, surface plasmon resonance (SPR) assays were employed to investigate the affinity between CQ and purified NLRP3 protein. The SPR assay revealed a high-affinity interaction between CQ and NLRP3 proteins, with an equilibrium dissociation constant (K_D) of 9.926 μmol/L (Fig. 6G). NLRP3 comprises three distinct domains: PYD, NACHT, and LRR. To identify the specific domain targeted by CQ, plasmids encoding different domains were generated and DARTS assays were performed on plasmid-transfected HEK-293T cells. Only the NACHT domain of NLRP3 exhibited protection against pronase upon CQ treatment (Fig. 6H).

To further elucidate CQ's mechanism in inhibiting NLRP3 activation, two mutant forms of NLRP3, NLRP3(R335A) and NLRP3(R335K), were constructed for DARTS experiments. Unlike the wild-type NLRP3, these mutants did not receive protection from pronase in the presence of CQ (Fig. 6I), indicating that CQ's anti-inflammasome activity involves direct binding to NLRP3. Additionally, CQ failed to inhibit the interaction between NLRP3(R335A/R335K)-NEK7 and ASC in transfected HEK-293T cells (Fig. 6J). Furthermore, CQ inhibited NLRP3 inflammasome activation in wild-type BMDMs but not in Nlrp3$^{-/-}$ BMDMs reconstituted with mutant NLRP3 (ARG-335A/K) (Figs. 6K–M).

These observations collectively support that CQ directly binds to a specific component of the NLRP3 inflammasome to suppress its assembly and activation. Therefore, CQ exhibits a strong protective effect on NLRP3 protein, with ARG-335 being a pivotal target for this interaction.

3.6. CQ prevents MSU-induced acute peritonitis

To investigate the effects of CQ on NLRP3 inflammasome activation, MSU crystals were used to induce a pro-inflammatory response associated with the progression of acute peritonitis [21]. C57BL/6 mice (6–8 weeks old) received injections of CQ or MCC950 before MSU at 12 h intervals. After 24 h, cells from the peritoneal cavity were collected for flow cytometry analysis. Results showed that CQ significantly reduced the frequency and number of white blood cells, neutrophils, and monocytes compared to DMSO-treated control mice (Figs. 7A and B). Although the relative percentage of macrophages did not differ significantly, consistent variations in absolute numbers were observed as expected (Fig. S4). CQ treatment also dose-dependently decreased NLRP3-induced IL-1β, IL-6, and TNF-α release (Fig. 7C). Immunoblot analysis demonstrated that CQ reduced the cleavage levels of caspase-1, IL-1β, and GSDMD (Fig. 7D). We also incorporated the combination of MCC950, a specific inhibitor of NLRP3, and CQ into the peritonitis mouse model to validate the specific role of CQ in peritonitis (Fig. S5). These data indicate that CQ effectively prevents MSU-induced NLRP3 inflammasome activation and mitigates acute peritonitis *in vivo*.

3.7. CQ significantly improves MSU-induced gouty arthritis

To evaluate CQ's therapeutic potential for MSU-induced gouty arthritis, foot thickness was measured at hourly intervals over 6 h post-MSU treatment. MSU was injected into the right foot, with PBS as a control in the left foot. The differential in foot thickness between the feet served as a metric for swelling. As anticipated, MSU injection induced significant footpad swelling, which was notably suppressed by CQ treatment (Fig. 8A). CQ pre-treatment resulted in a marked reduction in foot swelling duration compared to vehicle controls (MSU + DMSO) (Figs. 8B and C). Histological analysis of footpad tissues via H&E staining indicated that 10 mg/kg CQ mitigated inflammatory cell migration, clearly visible in actual tissue images (Fig. 8D). Furthermore, foot tissues cultured in DMEM medium for 1 h showed that CQ significantly decreased IL-1β levels (Fig. 8E) and caspase-1 activity (Fig. 8F) in treated mice. The classical NLRP3 inhibitor MCC950 (10 mg/kg) served as a comparative efficacy benchmark, confirming that CQ effectively mitigates gouty arthritis through its anti-inflammatory properties.

3.8. CQ delays the progression of sepsis induced by LPS

Sepsis, a severe bacterial infection, involves the initiation of systemic inflammation and subsequent organ dysfunction. Excessive activation of the NLRP3 inflammasome exacerbates pro-inflammatory responses, contributing to multiple organ failure and mortality during the acute phase of sepsis [22]. Mice were intraperitoneally administered LPS and continuously monitored for 72 h, CQ treatment significantly prolonged the survival time of septic mice (Fig. 9A). At the same time, there was no significant difference observed in the survival curve between mice administered with MCC950 and CQ in combination, and those administered with either MCC950 or CQ alone (Fig. S6). Flow cytometry analysis of blood cells in septic mice revealed no significant differences in the relative percentages or absolute numbers of white blood cells, macrophages, CD4$^+$ T cells, or CD8$^+$ T cells (Fig. S7). However, significant differences in the absolute numbers of neutrophils and monocytes were observed (Fig. 9B). H&E staining indicated pathological injury and inflammatory cell infiltration in lung and liver tissues, which improved following CQ treatment (Fig. 9C). ELISA analysis showed reduced levels of inflammatory cytokines IL-1β, IL-6, and TNF-α in the serum and lung tissues of CQ-treated mice (Figs. 9D and E). Additionally, Western blot analysis of lung tissue proteins demonstrated a significant decrease in the expression of cleaved caspase-1 p20 and IL-1β p17 in CQ-treated mice (Fig. 9F), indicating an attenuation in the release of these inflammatory factors and an improvement in sepsis progression.

3.9. CQ prevents DSS-induced colitis

The UC mouse model effectively replicates human IBD, enabling the study of pathogenesis and treatment through inducers like DSS and trinitrobenzene sulfonic acid solution (TNBSA). Disease severity is evaluated by monitoring weight, faecal characteristics, tissue pathology, and inflammatory mediators [23]. In this study, DSS-induced UC models were employed to further validate CQ's

Fig. 9. Clioquinol (CQ) alleviates lipopolysaccharide (LPS)-induced sepsis progression. 8–10 weeks C57BL/6 male mice were pre-injected with or without CQ/MCC950 (i.p) twice, and then injected with LPS (i.p) for 12 h. (A) The survival percentage of mice was monitored every 6 h until 72 h after LPS injection. (B) The percentage and number of neutrophils (CD 11B$^+$ Ly6G$^+$) and monocytes (CD 11B$^+$ Ly6C$^+$) in the peripheral blood of mice were detected by flow cytometry. (C) Representative hematoxylin and eosin (H&E) staining of mice lung and liver. (D, E) The interleukin (IL)-1β, IL-6 and tumor necrosis factor-α (TNF-α) levels in blood serum (D) and lung tissues (E). (F) NOD-like receptor protein 3 (NLRP3)-related protein expression in lung tissues. Data are representative of $n = 7$ (A, B, D), $n = 4$ (E), and are expressed as mean ± standard error of the mean (SEM). $^*P < 0.05$, $^{**}P < 0.01$, $^{***}P < 0.001$, ns: not significant, determined by analysis of variance (ANOVA), Wilcoxon test, Student's *t*-test or Mann–Whitney test (relative to LPS + dimethyl sulfoxide (DMSO)). ASC: apoptosis-associated speck-like protein containing a caspase activation and recruitment domain (CARD); GAPDH: glyceraldehyde phosphate dehydrogenase.

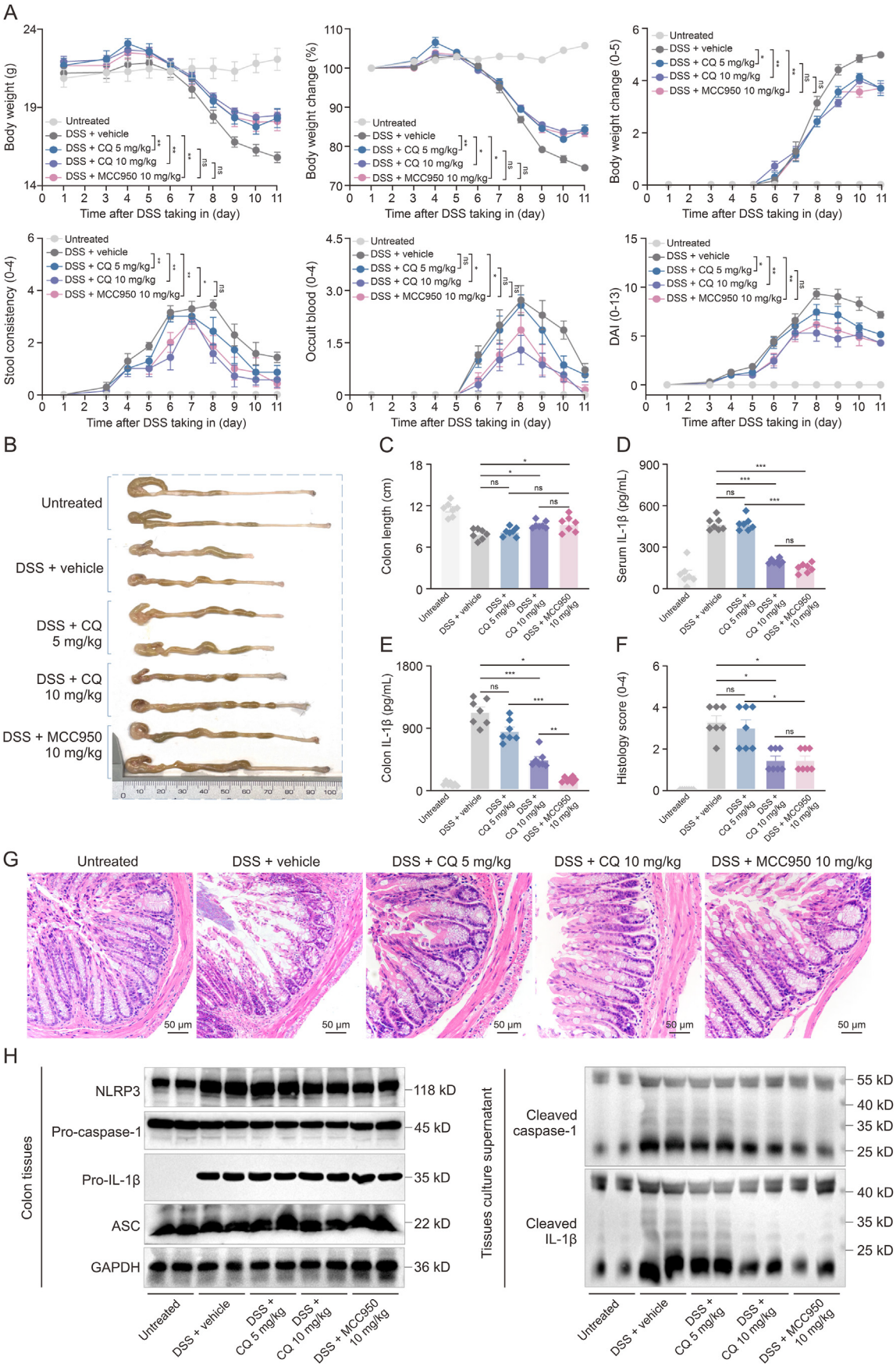
A
Body weight (g)
Body weight change (%)
Body weight change (0-5)
Stool consistency (0-4)
Occult blood (0-4)
DAI (0-13)
Time after DSS taking in (day)
Untreated
DSS + vehicle
DSS + CQ 5 mg/kg
DSS + CQ 10 mg/kg
DSS + MCC950 10 mg/kg
B
Untreated
DSS + vehicle
DSS + CQ 5 mg/kg
DSS + CQ 10 mg/kg
DSS + MCC950 10 mg/kg
C
Colon length (cm)
D
Serum IL-1β (pg/mL)
E
Colon IL-1β (pg/mL)
F
Histology score (0-4)
G
Untreated
DSS + vehicle
DSS + CQ 5 mg/kg
DSS + CQ 10 mg/kg
DSS + MCC950 10 mg/kg
50 μm
H
Colon tissues
NLRP3
Pro-caspase-1
Pro-IL-1β
ASC
GAPDH
118 kD
45 kD
35 kD
22 kD
36 kD
Tissues culture supernatant
Cleaved caspase-1
Cleaved IL-1β
55 kD
40 kD
35 kD
25 kD
40 kD
35 kD
25 kD

pharmacological effects. Over an 11-day observation period, CQ dose-dependently mitigated weight loss and improved faecal consistency, faecal blood, and the DAI score in colitis mice (Fig. 10A). By day 11, colon shortening was significantly alleviated in mice treated with CQ or MCC950 (Figs. 10B and C), and IL-1β levels in serum and colon tissues were reduced (Figs. 10D and E). CQ-treated mice exhibited reduced immune cell infiltration, fibrosis, mucosal ulceration, goblet cell loss, epithelial damage, and lower histological scores in colon tissue (Figs. 10F and G). Consistent with previous results, CQ demonstrated therapeutic and preventive effects comparable to MCC950 at the same dose. Western blot analysis of colon proteins corroborated these findings (Fig. 10H). These results indicate that CQ effectively alleviates DSS-induced UC in mice.

4. Discussion

This study identifies CQ as a promising candidate drug with potent anti-inflammatory effects. CQ effectively inhibited the activation of the NLRP3 inflammasome and subsequent NLRP3-mediated pyroptosis in both murine and human cells, evidenced by reduced caspase-1 processing, cytokine secretion, and pyroptotic cell death. Mechanistically, CQ specifically targeted NLRP3, exhibiting excellent inhibitory activity against IL-1β, with an IC_{50} value of 0.478 μM in BMDMs. CQ also suppressed the assembly of the NLRP3 inflammasome by interfering with the formation of the NLRP3-NEK7 complex and directly binding to the ARG335 residue in the NACHT domain of NLRP3. Animal studies confirmed that CQ alleviated NLRP3-mediated acute inflammation in mouse models of gouty arthritis, UC, and sepsis. These results collectively unveil a novel inhibitor targeting NLRP3 inflammasome activation, presenting a promising compound for therapeutic interventions against inflammatory diseases.

Abnormal activation of the NLRP3 inflammasome has been implicated in various human inflammatory diseases, including atherosclerosis [5], colitis [24], diabetes [25], AD [26], multiple sclerosis [27], and posttraumatic stress disorder [28]. CQ has shown potential therapeutic applications in neurodegenerative disorders such as Alzheimer's and Parkinson's disease [6,29–31]. Previous studies have demonstrated that CQ can induce autophagy, with its effects varying across different disease models [32,33]. Additionally, CQ may target the mTOR signalling pathway and alleviate lung fibrosis through iron chelation [12]. The role of CQ in inflammatory diseases has remained unclear until now. This study demonstrates CQ's potential to ameliorate inflammatory diseases by inhibiting NLRP3-mediated inflammation.

MCC950, the first identified NLRP3-specific inhibitor, has shown significant therapeutic benefits for inflammatory diseases [6]. Tranilast inhibits inflammasome activation by targeting the NACHT domain and preventing NLRP3 self-oligomerization. Recent studies have discovered that Tau protein directly acetylates specific sites (K21, K22, and K24) within the PYD domain of NLRP3, leading to *in vitro* activation of the NLRP3 inflammasome [34]. Additionally, post-translational palmitoylation occurs on the zinc finger structure within the LRR domain of NLRP3 through cellular metabolite palmitate and the ZDHHC5 enzyme, promoting the assembly and activation of the NLRP3 inflammasome [35]. In monocytes, nuclear translocation of NCOA6 binds to the ATP hydrolysis motif within the NACHT domain of NLRP3, promoting oligomerization with ASC and subsequent activation of NLRP3 inflammasomes [36]. Compared to other specific small molecule drugs targeting NLRP3 [6,8,34,35,37–42], CQ demonstrated superior efficacy against cellular pyroptosis. Unlike other studies reporting CQ-induced autophagy [32,33], this study confirmed that CQ inhibits the NLRP3 inflammasome independently of the autophagic pathway, specifically targeting NLRP3. Findings indicate that CQ binds to the NACHT domain of NLRP3, emphasizing its significance as a pharmacological target. The ATPase activity is essential for ASC association and NLRP3 oligomerization; therefore, inhibiting the ATP function of NLRP3 could lead to the development of effective inhibitors. Notably, CQ irreversibly suppresses the ATPase activity of NLRP3, surpassing current inhibitors in terms of efficacy. This may explain CQ's ability to effectively block the interaction between NEK7 and NLRP3, positioning it as a promising target for inhibitor development. However, further structural biology studies are required to fully elucidate the specific function of the NACHT domain. Molecular docking analysis predicted that CQ binds to the ARG335 residue of the NACHT domain, and subsequent experiments demonstrated that mutations at this site affect both the binding between NLRP3 and NEK7 and IL-1β expression levels. Nonetheless, further exploration into the role of the ARG335 site remains limited. Additionally, the precise molecular mechanism underlying CQ's inhibition of NLRP3 via this signalling pathway remains unexplored in depth within the scope of this study.

CQ exhibits promising therapeutic effects across various NLRP3-related disease models, demonstrating comparable efficacy to the classic NLRP3 inhibitor MCC950. Initial evaluations focused on CQ's capacity to impede NLRP3 inflammasome activation *in vivo*, utilizing models of acute peritonitis and gouty arthritis induced by MSU. Findings revealed that CQ effectively mitigates peritonitis and reduces intra-abdominal inflammatory cells and inflammatory factor levels. In osteoarthritis (OA), a disease characterized by joint cartilage degeneration, CQ treatment was associated with enhanced chondrocyte autophagy. Additionally, CQ promotes the expression of extracellular matrix (ECM) components while inhibiting inflammatory mediators, thereby improving the OA-associated microenvironment. In a rabbit model of trauma-induced OA, intra-articular injection of CQ effectively prevents or slows disease progression [43]. Similarly, in MSU-induced arthritis, CQ treatment effectively prevents disease progression, with treated tissues exhibiting reduced levels of IL-1β and Caspase-1. Further studies demonstrated that CQ inhibits the production of IL-1β, IL-6, and TNF-α in LPS-induced acute inflammation models, thereby extending the survival time of septic mice. The pharmacological effect of CQ on DSS-induced UC in mice was also investigated. UC, a chronic inflammatory disorder affecting the colonic mucosa, is mediated by the NLRP3 inflammasome and its signalling molecules [44]. CQ was found to alleviate DSS-induced UC and prevent the activation of the NLRP3 inflammasome in colon macrophages and dendritic cells. These outcomes align with previous reports demonstrating the efficacy of MCC950 and tranilast in reducing

Fig. 10. Clioquinol (CQ) prevents dextran sulfate sodium salt (DSS)-induced colitis. 8–10 weeks old C57BL/6 male mice were treated with 4% DSS for 8 day and then sterile water for additional 3 day. CQ (i.p) was injected from day 3. (A) Body weight, body weight change, stool consistency, occult blood and disease activity index (DAI) score were evaluated every day after DSS taking in. (B) Typical appearances of colon. (C) The colon length of ulcerative colitis (UC) mice on day 11. (D, E) The interleukin-1 beta (IL-1β) levels in blood serum (D) and colon tissues (E). (F, G) Mice colon sections were stained by hematoxylin and eosin (H&E) (F), and the statistical analysis of histology scores (G). (H) NOD-like receptor protein 3 (NLRP3)-related protein expression in colon tissues and culture supernatant. Data are representative of $n = 7$ (A, C–F), and are expressed as mean ± standard error of the mean (SEM). $^{*}P < 0.05$, $^{**}P < 0.01$, $^{***}P < 0.001$, ns: not significant, determined by two-way analysis of variance (ANOVA) (A), one-way ANOVA (C, D) or Wilcoxon test (E, F) (relative to DSS + DMSO). ASC: apoptosis-associated speck-like protein containing a caspase activation and recruitment domain (CARD); GAPDH: glyceraldehyde phosphate dehydrogenase; DMSO: dimethyl sulfoxide.

intestinal damage and increasing colon length in DSS-induced UC mice [7,8]. However, in sepsis, CQ did not significantly impact the relative proportions of neutrophils and monocytes but did affect absolute cell counts. This discrepancy may be attributed to suboptimal LPS dosage or inadequate sample collection timing, resulting in insufficient immunosuppressive effects.

5. Conclusions

NLRP3 inflammasomes and pyroptosis are crucial in regulating inflammation and immune responses. The complex interaction between NLRP3 and pyroptosis dictates cellular survival and death. Further investigation will elucidate the mechanisms governing NLRP3 inflammasome activation and cell death, providing insight into disease pathogenesis and innovative strategies for managing inflammatory disorders. Repurposing existing drugs and employing innovative adaptation strategies can significantly expedite drug development cycles, reduce research costs, and better meet medical demands. Discovering new therapeutic applications for established medications can mitigate risks associated with research uncertainty while addressing treatment challenges posed by rare or specialized diseases, offering patients more precise medical interventions. Our findings suggest that CQ has promising potential as a novel therapeutic agent for treating NLRP3-related diseases, providing a robust theoretical basis for its clinical application.

CRediT authorship contribution statement

Peipei Chen: Writing – original draft, Visualization, Validation, Software, Methodology, Investigation, Formal analysis, Data curation. **Yunshu Wang:** Project administration, Methodology, Investigation. **Huaiping Tang:** Methodology, Investigation. **Chao Zhou:** Writing – review & editing, Writing – original draft. **Zhuo Liu:** Funding acquisition. **Shenghan Gao:** Formal analysis. **Tingting Wang:** Writing – review & editing. **Yun Xu:** Funding acquisition, Conceptualization. **Sen-Lin Ji:** Writing – review & editing, Writing – original draft, Supervision, Project administration, Funding acquisition, Conceptualization.

Declaration of competing interest

The authors declare that there are no conflicts of interest.

Acknowledgments

This research was supported by the National Natural Science Foundation of China (Grant Nos.: 82101417, 81920108017, and 82130036), the STI2030-Major Projects (Project No.: 2022ZD0211800), Jiangsu Province Key Medical Discipline (Grant No.: ZDXK202216), the Key Research and Development Program of Jiangsu Province of China (Program No.: BE2020620), and Nanjing Medical Science and technology development Foundation, China (Grant No.: YKK20061). We would like to thank Editchecks (https://editchecks.com.cn/) for providing linguistic assistance during the preparation of this manuscript.

Appendix A. Supplementary data

Supplementary data to this article can be found online at https://doi.org/10.1016/j.jpha.2024.101069.

References

[1] E.I. Elliott, F.S. Sutterwala, Initiation and perpetuation of NLRP3 inflammasome activation and assembly, Immunol. Rev. 265 (2015) 35–52.
[2] K.V. Swanson, M. Deng, J.P.Y. Ting, The NLRP3 inflammasome: Molecular activation and regulation to therapeutics, Nat. Rev. Immunol. 19 (2019) 477–489.
[3] Y. Huang, W. Xu, R. Zhou, NLRP3 inflammasome activation and cell death, Cell. Mol. Immunol. 18 (2021) 2114–2127.
[4] X. Zhan, Q. Li, G. Xu, et al., The mechanism of NLRP3 inflammasome activation and its pharmacological inhibitors, Front. Immunol. 13 (2023), 1109938.
[5] P. Duewell, H. Kono, K.J. Rayner, et al., NLRP3 inflammasomes are required for atherogenesis and activated by cholesterol crystals, Nature 464 (2010) 1357–1361.
[6] R.A. Cherny, C.S. Atwood, M.E. Xilinas, et al., Treatment with a copper-zinc chelator markedly and rapidly inhibits β-amyloid accumulation in Alzheimer's disease transgenic mice, Neuron 30 (2001) 665–676.
[7] J. Li, L. Zhuang, X. Luo, et al., Protection of MCC950 against Alzheimer's disease via inhibiting neuronal pyroptosis in SAMP8 mice, Exp. Brain Res. 238 (2020) 2603–2614.
[8] A.P. Perera, R. Fernando, T. Shinde, et al., MCC950, a specific small molecule inhibitor of NLRP3 inflammasome attenuates colonic inflammation in spontaneous colitis mice, Sci. Rep. 8 (2018), 8618.
[9] R. Wykowski, A.M. Fuentefria, S.F. de Andrade, Antimicrobial activity of clioquinol and nitroxoline: A scoping review, Arch. Microbiol. 204 (2022), 535.
[10] D. Kaur, F. Yantiri, S. Rajagopalan, et al., Genetic or pharmacological iron chelation prevents MPTP-induced neurotoxicity in vivo, Neuron 37 (2003) 899–909.
[11] T. Nguyen, A. Hamby, S.M. Massa, Clioquinol down-regulates mutant huntingtin expression in vitro and mitigates pathology in a Huntington's disease mouse model, Proc. Natl. Acad. Sci. USA 102 (2005) 11840–11845.
[12] S. Lu, Y. Ke, C. Wu, et al., Radio sensitization of clioquinol and zinc in human cancer cell lines, BMC Cancer 18 (2018), 448.
[13] X. Lv, Z. Fan, F. Cao, et al., Clioquinol induces autophagy by down-regulation of calreticulin in human neurotypic SH-SY5Y cells, Chem. Biol. Interact. 369 (2023), 110268.
[14] A.I. Bush, Drug development based on the metal's hypothesis of Alzheimer's disease, J. Alzheimers Dis. 15 (2008) 223–240.
[15] C. Chen, Y. Zhou, X. Ning, et al., Directly targeting ASC by lonidamine alleviates inflammasome-driven diseases, J. Neuroinflammation 19 (2022), 315.
[16] R. Yuan, W. Zhao, Q. Wang, et al., Cucurbitacin B inhibits non-small cell lung cancer in vivo and in vitro by triggering TLR4/NLRP3/GSDMD-dependent pyroptosis, Pharmacol. Res. 170 (2021), 105748.
[17] Y. Huang, H. Jiang, Y. Chen, et al., Tranilast directly targets NLRP3 to treat inflammasome-driven diseases, EMBO Mol. Med. 10 (2018), e8689.
[18] J. Fu, H. Wu, Structural mechanisms of NLRP3 inflammasome assembly and activation, Annu. Rev. Immunol. 41 (2023) 301–316.
[19] S. Li, Y. Sun, M. Song, et al., NLRP3/caspase-1/GSDMD-mediated pyroptosis exerts a crucial role in astrocyte pathological injury in mouse model of depression, JCI Insight 6 (2021), e146852.
[20] M.Y. Pai, B. Lomenick, H. Hwang, et al., Drug affinity responsive target stability (DARTS) for small-molecule target identification, Methods Mol. Biol. 1263 (2015) 287–298.
[21] V.G. Magupalli, R. Negro, Y. Tian, et al., HDAC6 mediates an aggresome-like mechanism for NLRP3 and pyrin inflammasome activation, Science 369 (2020), eaas8995.
[22] L.G. Danielski, A.D. Giustina, S. Bonfante, et al., The NLRP3 inflammasome and its role in sepsis development, Inflammation 43 (2020) 24–31.
[23] R. Ungaro, S. Mehandru, P.B. Allen, et al., Ulcerative colitis, The Lancet 389 (2017) 1756–1770.
[24] C. Bauer, P. Duewell, C. Mayer, et al., Colitis induced in mice with dextran sulfate sodium (DSS) is mediated by the NLRP3 inflammasome, Gut 59 (2010) 1192–1199.
[25] H.M. Lee, J.J. Kim, H.J. Kim, et al., Upregulated NLRP3 inflammasome activation in patients with type 2 diabetes, Diabetes 62 (2013) 194–204.
[26] M.T. Heneka, M.P. Kummer, A. Stutz, et al., NLRP3 is activated in Alzheimer's disease and contributes to pathology in APP/PS1 mice, Nature 493 (2013) 674–678.
[27] W. Barclay, M.L. Shinohara, Inflammasome activation in multiple sclerosis and experimental autoimmune encephalomyelitis (EAE), Brain Pathol. 27 (2017) 213–219.
[28] Y. Dong, S. Li, Y. Lu, et al., Stress-induced NLRP3 inflammasome activation negatively regulates fear memory in mice, J. Neuroinflammation 17 (2020), 205.
[29] H.S.G.R. Investigators, Safety, tolerability, and efficacy of PBT2 in Huntington's disease: A phase 2, randomised, double-blind, placebo-controlled trial, Lancet Neurol 14 (2015) 39–47.
[30] X. Han, S. Sun, Y. Sun, et al., Small molecule-driven NLRP3 inflammation inhibition via interplay between ubiquitination and autophagy: Implications for Parkinson disease, Autophagy 15 (2019) 1860–1881.
[31] Q. Huang, P. Yang, Y. Liu, et al., The interplay between alpha-Synuclein and NLRP3 inflammasome in Parkinson's disease, Biomed. Pharmacother. 168 (2023), 115735.
[32] Z. Huang, L. Wang, L. Chen, et al., Induction of cell cycle arrest via the p21, p27-cyclin E, A/Cdk2 pathway in SMMC-7721 hepatoma cells by clioquinol, Acta Pharm 65 (2015) 463–471.
[33] I. Tanida, T. Ueno, E. Kominami, LC3 and autophagy, Methods Mol. Biol. 445 (2008) 77–88.

[34] L. Zhang, Y. Gai, Y. Liu, et al., Tau induces inflammasome activation and microgliosis through acetylating NLRP3, Clin. Transl. Med. 14 (2024), e1623.
[35] S. Zheng, X. Que, S. Wang, et al., ZDHHC5-mediated NLRP3 palmitoylation promotes NLRP3-NEK7 interaction and inflammasome activation, Mol. Cell 83 (2023) 4570–4585.e7.
[36] K. Lee, B.K. Hong, S. Lee, et al., Nuclear receptor coactivator 6 is a critical regulator of NLRP3 inflammasome activation and gouty arthritis, Cell. Mol. Immunol. 21 (2024) 227–244.
[37] S. Chen, Y. Li, Y. You, et al., Theaflavin mitigates acute gouty peritonitis and septic organ injury in mice by suppressing NLRP3 inflammasome assembly, Acta Pharmacol. Sin. 44 (2023) 2019–2036.
[38] R.C. Coll, A.A.B. Robertson, J.J. Chae, et al., A small-molecule inhibitor of the NLRP3 inflammasome for the treatment of inflammatory diseases, Nat. Med. 21 (2015) 248–255.
[39] H. He, H. Jiang, Y. Chen, et al., Oridonin is a covalent NLRP3 inhibitor with strong anti-inflammasome activity, Nat. Commun. 9 (2018), 2550.
[40] J. Shao, W. Li, J. Sun, et al., Britannin as a novel NLRP3 inhibitor, suppresses inflammasome activation in macrophages and alleviates NLRP3-related diseases in mice, Acta Pharmacol. Sin. 45 (2024) 803–814.
[41] G. Xu, S. Fu, X. Zhan, et al., Echinatin effectively protects against NLRP3 inflammasome-driven diseases by targeting HSP90, JCI Insight 6 (2021), e134601.
[42] J. Zhao, H. Liu, Z. Hong, et al., Tanshinone I specifically suppresses NLRP3 inflammasome activation by disrupting the association of NLRP3 and ASC, Mol. Med. 29 (2023), 84.
[43] X. Wu, P. Xu, X. Shi, et al., Intra-articular injection of clioquinol ameliorates osteoarthritis in a rabbit model, Front. Med. 9 (2022), 1028575.
[44] L. Mao, A. Kitani, W. Strober, et al., The role of NLRP3 and IL-1β in the pathogenesis of inflammatory bowel disease, Front. Immunol. 9 (2018), 2566.